Vol. 640: 79–105, 2020
https://doi.org/10.3354/meps13277

MARINE ECOLOGY PROGRESS SERIES
Mar Ecol Prog Ser

Published April 23

Effects of resuspension of eastern oyster *Crassostrea virginica* biodeposits on phytoplankton community structure

Elka T. Porter[1,*], Eric Robins[1], Sarah Davis[2], Richard Lacouture[2], Jeffrey C. Cornwell[3]

[1]University of Baltimore, Yale Gordon College of Arts and Sciences, Baltimore, MD 21201, USA
[2]Patuxent Environmental and Aquatic Research Laboratory, Morgan State University, Saint Leonard, MD 20685, USA
[3]Horn Point Laboratory, University of Maryland Center for Environmental Science, Cambridge, MD 21613, USA

ABSTRACT: Anthropogenic disturbances in the Chesapeake Bay (USA) have depleted eastern oyster *Crassostrea virginica* abundance and altered the estuary's environment and water quality. Efforts to rehabilitate oyster populations are underway; however, the effect of oyster biodeposits on water quality and plankton community structure are not clear. In July 2017, we used 6 shear turbulence resuspension mesocosms (STURMs) to determine differences in plankton composition with and without the daily addition of oyster biodeposits to a muddy sediment bottom. STURM systems had a volume-weighted root mean square turbulent velocity of 1.08 cm s^{-1}, energy dissipation rate of ~0.08 cm^2 s^{-3}, and bottom shear stress of ~0.36–0.51 Pa during mixing-on periods during 4 wk of tidal resuspension. Phytoplankton increased their chlorophyll *a* content in their cells in response to low light in tanks with biodeposits. The diatom *Skeletonema costatum* bloomed and had significantly longer chains in tanks without biodeposits. These tanks also had significantly lower concentrations of total suspended solids, zooplankton carbon, and nitrite + nitrate, and higher phytoplankton carbon concentrations. Results suggest that the absence of biodeposit resuspension initiates nitrogen uptake for diatom reproduction, increasing the cell densities of *S. costatum*. The low abundance of the zooplankton population in non-biodeposit tanks suggests an inability of zooplankton to graze on *S. costatum* and negative effects of *S. costatum* on zooplankton. A high abundance of the copepod *Acartia tonsa* in biodeposit tanks may have reduced *S. costatum* chain length. Oyster biodeposit addition and resuspension efficiently transferred phytoplankton carbon to zooplankton carbon, thus supporting the food web in the estuary.

KEY WORDS: Biodeposit · Resuspension · Phytoplankton · Zooplankton · Oyster · STURM · Mesocosm · *Crassostrea virginica* · Plankton · *Skeletonema costatum* · *Acartia tonsa*

1. INTRODUCTION

Anthropogenic disturbances in the Chesapeake Bay, the largest estuary on the US Atlantic coast, have depleted the abundance of the eastern oyster *Crassostrea virginica* (Newell 1988) and increased nutrient loading and phytoplankton abundance (Ator et al. 2019, Harding et al. 2019, Murphy et al. 2019). Although efforts to rehabilitate the oyster population through restoration (Schulte & Burke 2014) and aquaculture (Williamson et al. 2015, Ray et al. 2015) are underway, the impacts of the production and deposition of biodeposits on water quality and plankton community structure have not been evaluated. The euryhaline, epibenthic, bivalve filter feeder *C. virginica* filters large volumes of water and efficiently filters particles larger than 3 µm from the water column (Haven & Morales-Alamo 1970). Large amounts

*Corresponding author: eporter@ubalt.edu

of feces and pseudofeces produced by oysters as biodeposits reflect a transport of particulate organic matter from the water column to the sediments (Jordan 1987). While it is generally assumed that oyster biodeposits remain in oyster reefs (Newell et al. 2005, Kellogg et al. 2013), recent studies suggest that biodeposits can be resuspended (Colden et al. 2016, Porter et al. 2018a) and transported by currents (Lund 1957, Widdows et al. 1998, Testa et al. 2015). Studies suggest that nutrient regeneration from bivalve biodeposits may outweigh the presumed beneficial removal of phytoplankton biomass by stimulating new phytoplankton blooms (Doering et al. 1986, Asmus & Asmus 1991, Souchu et al. 2001), at least in oligotrophic waters (Cranford et al. 2007), and that bivalve feeding can skew phytoplankton demography toward smaller species that are no longer eaten by bivalves (Souchu et al. 2001, Cranford et al. 2007, Jiang et al. 2019).

Historically, 3 factors have been used to explain the size structure of phytoplankton communities: turbulence (Petersen et al. 1998, Iversen et al. 2010, Fouilland et al. 2016), nutrient supply (Van Meerssche & Pinckney 2019), and grazing by herbivores (Lebour 1922, Harvey et al. 1935). Overall, small algae are better competitors for light and nutrients than larger algae (Riegman et al. 1993). The effects of increased mixing on phytoplankton biomass results from complex interactions between the nutrient dynamics, light environment, and organismal physiology and behavior (Petersen et al. 1998). Phytoplankton growth rates decrease with turbulence while grazing rates increase, especially at low and intermediate turbulence levels (Peters & Marrasé 2000). Previous experimental studies of mixing observed a variety of contradictory responses by phytoplankton (Kiørboe 1993, Estrada & Berdalet 1997, Fouilland et al. 2016) and zooplankton (Davis et al. 1991, Dower et al. 1997). Iversen et al. (2010) showed that chlorophyll *a* (chl *a*), primary production rates, and diatom and dinoflagellate abundance were positively correlated to turbulence, regardless of nutrient conditions, and that abundance of autotrophic flagellates and total phytoplankton were positively correlated to turbulence only when nutrients were added. Slow mixing times stimulated the development of a mixed community of flagellates and small diatoms while fast mixing conditions developed a large diatom-dominated community, which stayed suspended only with high rates of mixing (Fouilland et al. 2016). Theoretical and experimental evidence suggests that sinking rates increase with cell volume (Smayda & Boleyn 1966, Smayda & Bienfang 1983, Kiørboe 1993). Large non-motile cells have higher sinking rates, when mixing rates are low, resulting in loss from the mixed zone, while mixing allows these large species to remain in the water column (Kiørboe 1993). Other factors such as shape and geometry also affect settling (Durante et al. 2019). Nutrient additions enhanced the biomass of the algal <20 µm fraction and increased the proportion of diatoms at the expense of cyanobacteria and cryptophytes (Van Meerssche & Pinckney 2019). Diatoms were previously thought to be passive prey for copepods, the dominant mesozooplankton (Lebour 1922, Harvey et al. 1935). However, recent investigations reveal that phytoplankton exhibit defense mechanisms that negatively affect zooplankton (Pančić & Kiørboe 2018), and these can include physiological characteristics (e.g. toxicity, bioluminescence), morphological characteristics (e.g. silica shell, colony formation), and behavioral defenses (e.g. escape response) (Pančić & Kiørboe 2018).

This study examines effects of oyster biodeposits and benthic boundary-layer flow on benthic–pelagic coupling processes as well as the phytoplankton and mesozooplankton community in a controllable whole-ecosystem context. The specific questions addressed were (1) How do resuspended biodeposits and their nutrients affect phytoplankton abundance and composition in mesocosm experiments with high bottom shear and realistic water column turbulence? (2) How does oyster biodeposit resuspension affect ecosystem processes such as the mesozooplankton community? These experiments were designed to determine if the combined effect of high bottom shear stress with tidal resuspension of sediments and oyster biodeposits directly, indirectly, or non-linearly impacts ecological interactions and water quality. Particular emphasis was placed on understanding the effect of biodeposit addition and resuspension on changes in the phytoplankton and mesozooplankton community structure and biomass in the ecosystem.

2. MATERIALS AND METHODS

2.1. Mesocosm setup and mixing

In June and July 2017, 6 cylindrical shear turbulence resuspension mesocosm (STURM; Porter et al. 2018b) tanks were set up at the Patuxent Environmental and Aquatic Research Laboratory (PEARL), Morgan State University, in St. Leonard, Maryland (USA), with a ~10 cm deep muddy sediment bottom,

covered by pre-screened, unfiltered Chesapeake Bay water from the Patuxent estuary. STURM systems contain a single paddle that produces high instantaneous bottom shear stress to resuspend biodeposits and sediment, with realistic water column turbulence levels without overmixing the water column (Porter et al. 2018b). The STURM tanks are the successor design of large linked mesocosms reported by Porter et al. (2004a,b). The tanks have a water volume of 1000 l, a water column depth of 1 m, and a sediment surface area of 1 m^2. Paddle speed was set to 12.5 rpm, and a single paddle slowly moved in a forward-stop-backward-stop motion (9 s – 1.5 s – 8 s – 1.5 s) to avoid plug flow during the mixing-on phase. Mixing followed a 4:2 h on:off cycle in all systems to simulate tidal cycles throughout a 4 wk experiment.

Direct flow and turbulence measurements were made using an acoustic Doppler velocimeter to determine water column root mean square (RMS) turbulent velocities and energy dissipation rates at predefined locations throughout the tank, and at different mixing speeds. RMS turbulent velocity (cm s^{-1}) was defined by Tennekes & Lumley (1972) as:

$$q = \sqrt{\frac{1}{3}(<u^2> + <v^2> + <w^2>)} \quad (1)$$

where $<u^2>$, $<v^2>$, and $<w^2>$ are the variances of their respective velocity components. Energy dissipation rates (cm^2 s^{-3}) were determined following Sanford (1997). Volume-weighted RMS turbulent velocities as determined using Surfer (Golden Software) were approximately 1.08 cm s^{-1} (Fig. 1a), and volume-weighted energy dissipation rates were approximately 0.0772 cm^2 s^{-3} during mixing-on (Fig. 1b); this is similar to the intermediate mixing treatment of Petersen et al. (1998). These turbulence levels are comparable to ones used in resuspension tanks in previous experiments comparing resuspension vs. non-resuspension systems (Porter et al. 2010), and in linked mesocosms (Porter et al. 2004a,b), lower than used by Porter et al. (2018a), and are in a realistic range (Porter et al. 2018b; see Table 1 in Sanford 1997). In addition, this mixing setting kept energy dissipation rates at realistic Chesapeake Bay levels.

Shear stress at the bottom was determined directly using hot-film anemometry (Gust 1988). Shear (or 'friction') velocity ($u_\star$ in cm s^{-1}) is defined by:

$$u_\star = \sqrt{\frac{\tau_b}{\rho}} \quad (2)$$

where τ_b is bottom shear stress in dynes cm^{-2} and ρ is the density of water in g cm^{-3}, and was measured at 5 locations across the tank radius. Bottom shear stress (measured in Pa) was calculated as:

$$\tau_b = \frac{u_\star^2 \rho}{10} \quad (3)$$

At the chosen mixing setting of 12.5 rpm, maximum instantaneous bottom shear stress reached 0.36–0.51 Pa in all tanks (Fig. 1c; Porter et al. 2018b) and produced resuspension of biodeposits and sediments in the tanks during the mixing-on phases.

The mesocosms were prepared with muddy sediment, collected on 7 June 2017, from the mesohaline Patuxent estuary (38° 22′ 0.9″ N, 76° 30′ 0.7″ W), a tributary of the Chesapeake Bay. Sediment was transported to PEARL where it was placed in outdoor mesocosms on 12 June after anaerobic defaunation (Porter et al. 2006). The sediment was equilibrated to realistic biogeochemical pore water gradients in the dark over a 2 wk period with a 30 cm water column of 0.5 µm filtered Patuxent estuary water (PEW) as described by Porter et al. (2006) (called Treatment HG-m in that study) (Porter et al. 2010, 2013). During the sediment equilibration phase in the dark, the partial water column was oxygenated, and 50% of the 0.5 µm filtered PEW in the tanks was replaced daily with 0.5 µm filtered PEW for 2 wk. At the end of the sediment equilibration period, tanks were emptied and filled to 1 m water column height with unfiltered ambient PEW. Each day, 10% of the water in each tank was exchanged during the mixing-off phase and replaced with 0.5 µm absolute filtered PEW to mimic tidal exchange and without introducing a new plankton community.

During mixing-on, 3 tanks each received a daily addition of oyster biodeposits starting after the first water column sampling. Thus, Day 1 of sampling, i.e. time 0, is excluded in all data analyses except where the initial phytoplankton biomass is compared to the experimental phytoplankton biomass. During the Day 1 afternoon mixing-on phase, each tank received 62 g of biodeposits in addition to the ambient resuspended total suspended solids (TSS) in the tanks to get started. On all subsequent days, 4.76 ± 2.93 g (SD) TSS from biodeposits were added daily to each tank. Biodeposits from oysters feeding on natural plankton from the Patuxent estuary were generated in an indoor raceway in continuous flow conditions. TSS, particulate inorganic matter (PIM), particulate organic matter (POM), and quality (ratio of POM:PIM) of the added biodeposits were determined daily while particulate carbon (PC), particulate nitrogen (PN), chl *a*, and phaeophytin concentrations were determined in biodeposits every other day.

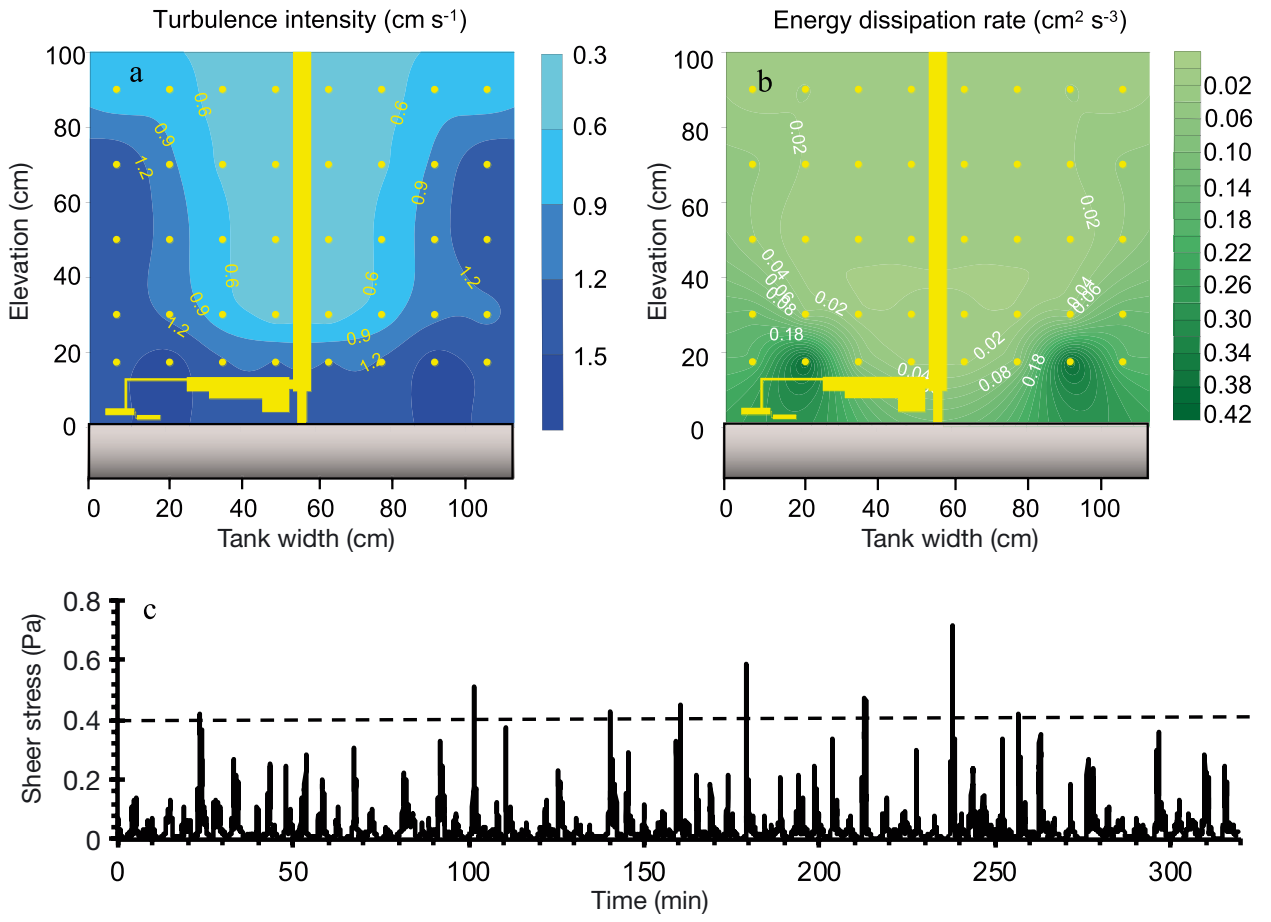

Fig. 1. (a) Turbulence intensity, (b) energy dissipation rate during a mixing-on phase in the resuspension (R) tanks and in the resuspension with daily biodeposit additions (R_BD) tanks. The R_BD tanks had daily additions of biodeposits over a 4 wk experiment. Yellow circles: measurement locations. Tidal cycles (4 h mixing on, 2 h mixing off) were generated in all tanks. (c) Bottom shear stress in the STURM tanks during a mixing-on phase

The STURM tanks were wrapped in reflective bubble wrap (Shelter Institute) to reduce overheating of the tank water during high outdoor summer temperatures (≤38°C). In addition, 2 layers of window screen mesh were placed over the superstructure to reduce insolation, ca. 1.5 m above the tanks. Light levels of ~356 µmol photons m^{-2} s^{-1} were measured at the water surface of the Resuspension (R) tanks and the Resuspension with biodeposit addition (R_BD) tanks, using an LI-192 Underwater Quantum sensor (LI-COR Biosciences) attached to a model LI-250 readout. Previous experiments indicate that light levels of about 160 µmol photons m^{-2} s^{-1} are required at the water surface to prevent light limitation (Porter et al. 2004a). Therefore, any light limitation within the tanks was due to the impact of sediment and biodeposit resuspension and the density of phytoplankton that resulted.

The tanks were slowly and evenly filled with prescreened, unfiltered 12.0 PSU salinity water containing the resident plankton community from the Patuxent estuary. Only megazooplankton >3 cm were excluded. Mixing began with the programmed tidal cycles, and all tanks were synchronized. The experiment took place from 26 June to 26 July 2017 (30 d). Rainstorms added fresh water to the tanks on experiment Days 10, 14, 18, and 27, each time reducing salinity from 12 to 10 PSU. On Day 25, the seams of the walls of one R_BD tank burst open and the tank was lost. The experiment continued with the 5 remaining tanks until Day 30, and the results from Days 25 through 30 were averaged from the remaining 2 R_BD tanks. During the evening of Day 10, a data acquisition failure in the mixing system caused the mixing in all systems to be off for 2 mixing-on phases. After fixing the issue (cable unplugged), the systems continued with no further problems until the end of the experiment. Following this event, researchers began constant remote monitoring of the systems using a remotely accessible status webpage

(Porter et al. 2018b). Using a separate cleaning stick for each tank to prevent tank cross-contamination, tank walls were cleaned of periphyton every day to minimize wall growth (Chen et al. 1997), and the wall material was left in the tank.

2.2. Sampling regime and variables sampled

Biological and geochemical variables measured included water column chl *a*, phaeophytin, TSS concentrations, phytoplankton identification and cell counts, phytoplankton pigment composition using high performance liquid chromatography (HPLC), and water column nutrient concentrations (ammonium, nitrate plus nitrite, dissolved inorganic nitrogen [DIN], phosphate, total dissolved nitrogen [TDN], total dissolved phosphorus [TDP]), with samples taken at mid-depth. In addition, light profiles, Secchi depth, and sediment chl *a* were determined. Finally, particle bulk settling speeds were measured during mid-day mixing-off phases in the R_BD and the R tanks using optical backscatter turbidity data.

In each tank, turbidity was continuously measured at 1 s intervals with optical backscatter turbidity sensors (OBS-3, D&A Instrument) located at mid-depth. Turbidity was calibrated with concurrently collected mid-depth TSS samples, analyzed by filtration and weighing as described by Porter et al. (2018a). Water temperatures were taken at 10 min intervals in all tanks using Campbell T107 temperature probes as in Porter et al. (2010, 2013, 2018a). A heat wave occurred during Days 18–19, and 26–28; however, water temperatures in the tanks were similar to water temperatures measured in a shallow local Patuxent estuary cove (31.2°C), making tank cooling intervention unnecessary. Silver bubble wrap and 2 layers of window screen above the tanks were sufficient to shield the tanks from excessive heat.

Twice a week, light profiles were measured during mixing-on and -off phases as described by Porter et al. (2018a) to determine irradiance levels at the bottom, and mean geometric irradiance in the water column was calculated as $\exp\{0.5 \times [\ln(E_0) + \ln(E_{Sed})]\}$, where E_0 and E_{Sed} are irradiances at the surface of the water column and the bottom, respectively. The values obtained for mean geometric irradiance were similar to irradiance values measured at 50 cm depth. Secchi depth was measured daily during the mixing-on and -off phases as in Porter et al. (2018a).

Water samples (4 l) were taken from mid-depth of each tank twice a week during mixing-on for measurements of particulates and solutes and on Days 15, 22, and 29, and at the end of the mixing-off phases. Water was filtered through 47 mm Whatman GFF filters (0.7 µm nominal pore size), and filters were analyzed for TSS, PIM, and POM as described by Porter et al. (2018a), following Berg & Newell (1986). Known volumes of water were filtered through 47 mm Whatman GFF filters, and filters were analyzed for particulate phosphorus (PP) concentrations, and chl *a* and phaeophytin concentrations. Water column chl *a* concentrations were analyzed using fluorometric techniques after extraction with 90% acetone (EPA Method 445.0) to provide estimates of phytoplankton biomass, where phaeophytin was measured fluorometrically following acidification. In addition, water was filtered through pre-washed 25 mm Whatman GFF filters to measure PN and PC concentrations. The solute was captured and frozen in individual vials until it was analyzed for dissolved nutrients including ammonium (NH_4^+), nitrate + nitrite (NO_3^- + NO_2^-), dissolved phosphate (PO_4^{3-}), dissolved silicate (Si), TDN, and TDP concentrations using analytical procedures outlined by Porter et al. (2018a). Dissolved organic nitrogen (DON) was calculated by subtracting NH_4^+ and NO_3^- + NO_2^- from TDN, and dissolved organic phosphorus (DOP) was calculated by subtracting PO_4^{3-} from TDP. Exchange water was also sampled for dissolved nutrients to track any nutrient inputs through a 10% daily water exchange. In addition, the fill water was sampled for particulates to confirm that their abundance in the 0.5 µm filtered fill water was low. The same techniques were used to analyze particulates in the biodeposits. For quality control of all variables, every sixth sample was analyzed in duplicate. Nutrients and water column chl *a* and phaeophytin were analyzed by the Analytical Services Laboratory of the Chesapeake Biological Laboratory, University of Maryland Center for Environmental Science (UMCES; water column chemistry methods and particulates methods at https://www.umces.edu/nasl/methods).

Samples for pigment analysis were collected from the mid-depth of each tank and stored in a –80°C freezer until analysis using HPLC (Van Heukelem & Thomas 2001). Following Jeffrey & Vesk (1997), Marshall (1994), and Marshall et al. (2005), some pigments characteristic of phytoplankton in the Chesapeake Bay area, our source water, were defined as alloxanthin (Cryptophyceae), fucoxanthin (Chrysophyceae and Bacillariophyceae), lutein (Chlorophyceae and Prasinophyceae), peridinin (Dinophyceae), zeaxanthin (cyanobacteria, prochlorophytes, rhodophytes, and some Chlorophyceae), neoxanthin (Chlorophyceae and Prasinophyceae), and prasinoxanthin (Prasino-

phyceae). The ratio of chl *b* to chl *a* was taken to indicate chlorophytes (Van Meerssche & Pinckney 2019). HPLC samples were analyzed by Analytical Services of the Horn Point Laboratory, UMCES.

Moreover, water subsamples were preserved biweekly in Lugol's iodine solution for later microscopic phytoplankton identification and cell counts. Phytoplankton cells were counted using Utermöhl procedures (Utermöhl 1958, Marshall & Alden 1990, Lacouture 2010), and 20 random fields were counted at 500× for most cells smaller than 10 µm. A minimum of 10 random fields and 200 individual cells were counted at 12.5 × 25 = 312.5×. A scan of the entire settling chamber was performed at 125×. The sample volume was 125 ml, and the subsample volume in the counting chamber was 2.5 ml. Phytoplankton biomass was determined by converting mean cell volumes of individual taxa to cell carbon according to Strathmann (1967) and Smayda (1978).

Phytoplankton biomass was estimated for 3 phytoplankton cell size ranges (cell volume 3–240, 241–6200, 6201–65 300 µm^3) to determine if phytoplankton size of the community changed over the experiment and in response to the treatments. Fluorescence microscopy (MacIsaac & Stockner 1993) and flow cytometry (Veldhuis & Kraay 2000) were not applied. Dissolved organic carbon (DOC) concentrations were similar in R tanks with 194.99 ± 56.09 µmol C l^{-1} (SD) and 205.58 ± 36.55 µmol C l^{-1} in R_BD tanks (p = 0.6628). To determine if the light regime in the R and R_BD tanks affected phytoplankton, the ratio of chl *a* to carbon was determined from the chl *a* concentration and total phytoplankton carbon determined from direct counts. Phytoplankton abundance at time zero (morning after the fill, before biodeposits were added) was compared to average phytoplankton abundance during the experiment (Days 2–29) to determine any change in the phytoplankton community from initial conditions. While counting *Skeletonema costatum* cells in the phytoplankton samples, *Skeletonema* chain length appeared to be longer in the R tanks than in the R_BD tanks, thus *S. costatum* chain length was determined across all tanks between Days 10 and 30.

During each water sampling, the exact times of sampling for each OBS-3 turbidity meter was recorded to establish linear calibration curves of TSS versus OBS volts (Table 1, p < 0.0001). The linear calibrations for each OBS-3 turbidity meter (Table 1) were used to determine TSS concentrations in the tanks from continuous OBS turbidity measurements. Bulk particle settling speed (mm s^{-1}) was measured in all tanks using the settling profiles generated by the OBS-3 turbidity meters during mixing-off phases. The distance from the surface to the turbidity sensor (0.5 m depth) was divided by the time to reduce the initial TSS concentration by 50% of the range to its steady state value. Bivalves repackage organic and inorganic matter into biodeposits, likely increasing the average size structure and settling of the particles in the R_BD tanks compared to R tanks. More frequent samples of TSS, PIM, POM, POM:PIM, PN, PP, PC, and chl *a* were also collected during 3 mixing-off periods on Days 15, 22, and 29 to examine changes in the particulate properties over time during settling.

Sediment chl *a* and sediment phaeophytin concentrations were measured at the end of the experiment and the samples were analyzed fluorometrically (Parsons et al. 1984). At time zero, no microphytobenthos was expected to be present, as the sediments had been kept in the dark during the sediment re-equilibration process after defaunation before STURM experiment start. Sediment cores were taken at the end of the experiment, the contents washed through a 0.5 mm diameter mesh, and the sample preserved with buffered formaldehyde; however, no macrofauna was found in any of the tanks.

2.3. Zooplankton

Mesozooplankton was sampled twice a week during mixing-off by pumping 40 l tank^{-1} at 27 l min^{-1} through a 63 µm Nitex screen using a diaphragm pump, and these samples were washed into bottles and preserved with buffered formaldehyde. Dominant taxa and age groups of the mesozooplankton were determined on a dissecting microscope using direct counts. To estimate the dry weights of all individuals of the different taxa, the number of individuals was multiplied by their taxon's respective dry weight (Table 2). Dry weight for polychaetes was

Table 1. Linear relationship of optical backscatter sensor volts (OBS3_V) and total suspended solids (TSS) concentrations in the 6 tanks. T1, T2, T6: resuspension tanks; T3, T4, T5: resuspension tanks with daily biodeposit additions

Tank	Regression	R^2	n	p
T1	TSS = 124.84 × OBS_V +17.756	0.91	12	<0.0001
T3	TSS = 216.32 × OBS_V + 36.359	0.97	12	<0.0001
T2	TSS = 323.12 × OBS_V + 23.282	0.95	12	<0.0001
T4	TSS = 193.51 × OBS_V + 36.697	0.96	7	<0.0001
T6	TSS = 350.43 × OBS_V + 18.433	0.98	10	<0.0001
T5	TSS = 95.04 × OBS_V + 44.444	0.88	12	<0.0001

Table 2. Dry weights (µg ind.$^{-1}$) of zooplankton used for conversions to zooplankton carbon. Small polychaetes in the experiment were ~0.152 mm and large polychaetes were ~0.536 mm long

Species	Dry weight	Reference
Acartia tonsa	8	White & Roman (1992)
Copepodites	2.7	White & Roman (1992)
Copepod nauplii	0.31	White & Roman (1992)
Barnacle nauplii	0.31	White & Roman (1992)
Rotifers (>63 µm)	1.2	White & Roman (1992)
Cyclopoid copepods	0.35	White & Roman (1992)
Other calanoid copepods	9.05	White & Roman (1992)
Veliger larvae	0.1342	Sprung (1984)
Small (~0.152 mm) polychaetes	2.1	White & Roman (1992)
Large (~0.536 mm) polychaetes	20.6	White & Roman (1992)
Harpacticoids	3.99	Goodman (1980)
Flatworms/Turbellaria	2	Faubel (1982)

determined from measured polychaete length (White & Roman 1992). The dominant taxa were copepod nauplii, *Acartia tonsa* adults, polychaete larvae, and copepodites. Zooplankton densities (no. l^{-1}) were converted to carbon (µg l^{-1}) for each taxon following White & Roman (1992, their Table 1: 'Carbon [µg C ind^{-1}] = 0.32 W'), and the taxa were combined for an estimate of combined mesozooplankton biomass to compare their relative biomass to phytoplankton biomass (in a common carbon unit).

2.4. Statistical analyses

The same statistical analyses were used as in Porter et al. (2010, 2013, 2018a). Chl *a*, phaeophytin, TSS, dissolved inorganic and organic nutrients, and PN, PP, and PC were each averaged from Days 2–29 of the experiment for each tank (8 measurements over a 4 wk period). An additional measurement on Day 1, while graphed, was not included in the statistical analysis as no biodeposits had yet been added to the R_BD tanks. For some variables, statistical analysis was performed only on data from Day 15 to the end of the experiment. A split plot design in SAS 8.2 was used for mixing-on–mixing-off particulate concentrations (PC, PN), on–off geometric mean irradiance, on–off irradiance at the sediment surface, as well as on–off water column chl *a* concentrations, phaeophytin concentrations, and ratio of chl *a* to phaeophytin. In addition, split plot in time in SAS 8.2 was used to compare the initial phytoplankton biomass to average biomass during Days 2–29. Post hoc tests for the split plot design were the Student Newman Keuls test and least squares means analyses in SAS 8.2.

Statistical *t*-tests were used to determine if there was a shift towards smaller phytoplankton cells (cell volume 3–240 µm^3) versus larger cells (241–65 300 µm^3) in the R and R_BD tanks, respectively.

Mesozooplankton abundance was averaged for each tank from Days 3–28. Only data from the mixing-on phases were included in statistical comparisons. Statistical *t*-tests were used for on-phase water column chl *a*, phaeophytin, PN, PC, dissolved nutrient data, dissolved oxygen, zooplankton abundance, and the sediment chl *a* data, water column accessory pigment to chl *a* ratios, and direct counts of phytoplankton abundance.

Linear regression of mesozooplankton biomass and phytoplankton biomass (estimated from direct cell counts) were used to determine the relationship between the mesozooplankton community and phytoplankton. Statistical *t*-tests and regression analyses were done using the Microsoft Excel Analysis ToolPak. All analyses were considered significant at $p \leq 0.05$. Unless indicated otherwise, values are given as means ± SD.

3. RESULTS

3.1. Biodeposits added

On average, 4.8 ± 2.9 g TSS, 478 ± 220 mg PC, 64.1 ± 33.4 mg PN, and 14.2 ± 8.6 mg PP in the biodeposits were added to each tank daily (Table 3) with a ratio of POM to PIM of 0.6 ± 0.3. With 2.73 ± 1.9 mg chl *a*, 6.63 ± 4.76 mg phaeophytin, small amounts of chl *a* were found in biodeposits and added to the tanks with the biodeposits daily. On the first day, in the afternoon mixing-on phase after sampling, 62.1 g TSS, 3 g PC, 398 mg PN, and 123.6 mg PP were added to each tank (Table 3).

3.2. Water column processes

Water temperatures ranged from 22.61 to 30.46°C in the experiment (R tanks: 27.24 ± 1.63°C; R_BD anks: 27.21 ± 1.67°C), and temperatures in the 6 tanks tracked each other closely ($p = 0.7498$, Fig. 2). Water temperatures were about 2.4°C cooler over the first part of the experiment from Days 0 to 15 than in the second part of the experiment (Day 15 to the end), during which the experiment experienced 2 heat waves.

Table 3. Summary of statistical results for the resuspension (R) and resuspension with biodeposit addition (R_BD) systems during the mixing-on phases. All systems contain muddy sediments. Statistical *t*-tests were used in all analyses. Significant differences ($p \leq 0.05$) are highlighted in **bold**. Included in the analysis were all days of the experiment except for Day 1 on which no biodeposits had been added yet to any systems. Sediment results are from the end of the experiment. Means ± SD, n = 3

Variable	R	R_BD	p	Days
Seston				
Total suspended solids (mg l^{-1})	137.40 ± 72.05	222.46 ± 58.71	**0.0225**	2–29
Particulate inorganic matter (PIM; mg l^{-1})	114.38 ± 64.62	182.73 ± 52.47	**0.0371**	2–29
Particulate organic matter (POM; mg l^{-1})	23.02 ± 7.71	39.73 ± 8.17	**0.0009**	2–29
Ratio POM:PIM	0.24 ± 0.07	0.23 ± 0.04	0.8908	2–29
Percent PIM	81.41 ± 4.02	81.33 ± 2.70	0.9618	2–29
Chl *a*, phaeophytin				
Chlorophyll *a* (µg l^{-1})	45.83 ± 26.70	44.61 ± 11.73	0.9085	2–29
Phaeophytin *a* (µg l^{-1})	23.51 ± 12.45	65.22 ±15.78	**<0.0001**	2–29
Ratio chl *a*:phaeophytin	1.97 ± 0.70	0.73 ± 0.17	**0.0013**	2–29
Ratio chl *a*:phytoplankton carbon	0.016 ± 0.007	0.046 ± 0.006	**0.0002**	2–29
Particulates				
Particulate phosphorus (µmol l^{-1})	5.56 ± 2.52	11.24 ± 2.49	**0.0005**	2–29
Particulate carbon (PC, mmol l^{-1})	0.49 ± 0.26	1.01 ± 0.20	**0.0006**	2–29
Particulate nitrogen (PN, µmol l^{-1})	55.74 ± 27.66	122.09 ± 22.24	**0.0025**	2–29
Ratio PC:PN	8.39 ± 0.88	8.23 ± 0.13	0.6214	2–29
Dissolved nutrients, dissolved organic carbon, dissolved oxygen				
Ammonium (µmol l^{-1})	0.51 ± 0.14	0.76 ± 0.67	0.3316	2–29
Nitrate + nitrite (µmol l^{-1})	2.88 ± 2.98	6.27 ± 3.12	**0.0433**	2–29
Total dissolved nitrogen (µmol l^{-1})	22.81 ± 4.97	27.27 ± 4.53	0.0816	2–29
Dissolved inorganic nitrogen (DIN, µmol l^{-1})	3.39 ± 3.09	7.03 ± 3.32	**0.0395**	2–29
Dissolved organic nitrogen (µmol l^{-1})	8.79 ± 1.30	9.16 ± 1.47	0.5998	2–29
Total dissolved phosphorus (µmol l^{-1})	0.56 ± 0.50	0.69 ± 0.45	0.6023	2–29
Soluble reactive phosphorus (SRP, µmol l^{-1})	0.35 ± 0.43	0.44 ± 0.40	0.6959	2–29
Dissolved organic phosphorus (µmol l^{-1})	0.21 ± 0.09	0.25 ± 0.08	0.3401	2–29
Dissolved organic carbon (µmol l^{-1})	194.99 ± 56.09	205.58 ± 36.55	0.6628	2–29
Dissolved silica (µmol l^{-1})	54.90 ± 29.14	50.22 ± 26.31	0.7410	2–29
Ratio DIN:SRP	19.01 ± 15.60	48.71 ± 69.83	0.2742	2–29
Ratio dissolved silicate:SRP	464.71 ± 296.40	360.61 ± 684.71	0.7014	2–29
Dissolved oxygen (mg l^{-1})	6.21 ± 1.01	4.00 ± 1.24	**<0.0001**	2–30
Total nutrients				
Total nitrogen (µmol l^{-1})	78.55 ± 23.78	149.36 ± 23.30	**<0.0001**	2–29
Total phosphorus (µmol l^{-1})	6.12 ± 2.15	10.82 ± 2.21	**0.0007**	2–29
Ratio total nitrogen:total phosphorus	13.30 ± 1.34	12.68 ± 0.60	0.2624	2–29
Zooplankton				
Adult *Acartia tonsa* (ind. l^{-1})	4.99 ± 3.45	52.32 ± 27.17	**0.0018**	3–28
Copepodites (ind. l^{-1})	2.11 ± 2.71	37.16 ± 59.82	0.1418	3–28
Copepod nauplii (ind. l^{-1})	70.67 ± 48.34	382.2 ± 387.5	0.0587	3–28
Polychaete larvae large (ind. l^{-1})	14.38 ± 10.80	15.43 ± 19.25	0.8953	3–28
Polychaete larvae small (ind. l^{-1})	21.43 ± 28.10	10.59 ± 21.32	0.4002	3–28
Veliger larvae (ind. l^{-1})	0.22 ± 0.27	0.33 ± 0.22	0.4048	3–28
Rotifers (>63 µm) (ind. l^{-1})	0.48 ± 1.06	57.94 ± 105.18	0.1662	3–28
Harpacticoid copepods (ind. l^{-1})	0.052 ± 0.061	0.372 ± 0.401	0.1515	3–28
Flatworms (ind. l^{-1})	0.092 ± 0.120	0.083 ± 0.138	0.1018	3–28
Nematodes (ind. l^{-1})	0.092 ± 0.120	0.083 ± 0.138	0.8949	3–28
Cyclopoid copepods (ind. l^{-1})	0.037 ± 0.033	0.029 ± 0.044	0.3776	3–28
Other calanoid copepods (ind. l^{-1})	0.046 ± 0.059	0.062 ± 0.078	0.5606	3–28
Zooplankton carbon (µg l^{-1})	131.4 ± 84.3	330.5 ± 230.8	**0.0476**	3–28
Sediment				
Percent carbon in top cm	3.17 ± 0.0656	3.35 ± 0.0006	**0.0403**	
Percent nitrogen in top cm	0.42 ± 0.0084	0.44 ± 0.0012	**0.0330**	
Percent dry weight	24.21 ± 0.27	22.18 ± 0.97	**0.0007**	
Sediment chl *a* (mg m^{-2})	42.51 ± 13.89	37.90 ± 9.65	0.5129	

Table 3 (continued)

Variable	R	R_BD	p	Days
Biodeposit additions				
Particulate carbon (mg C tank^{-1})		Day 1: 3036 mg All other days: 477.92 ± 219.99 mg d^{-1}		
Particulate nitrogen (mg N tank^{-1})		Day 1: 397.8 mg All other days: 64.05 ± 33.39 mg d^{-1}		
Particulate phosphorus (mg P tank^{-1})		Day 1: 123.6 mg All other days: 14.22 ± 8.57 mg d^{-1}		
Chl *a* (mg chl *a* tank^{-1})		Day 1: 7.2 mg All other days: 2.73 ± 1.9 mg d^{-1}		
Phaeophytin (mg phaeophytin tank^{-1})		Day 1: 19.8 mg All other days: 6.6 ± 4.76 mg d^{-1}		

TSS concentrations were significantly higher in the tanks with oyster biodeposits (R_BD; 222.46 ± 58.71 mg l^{-1}; Fig. 3, Table 3) than in the resuspension tanks without added biodeposits (137.4 ± 72.05 mg l^{-1}, p = 0.0225, Days 2–29; Fig. 3, Table 3). TSS in R tanks came from resuspended bottom sediment, TSS in R_BD tanks came from resuspended bottom sediment plus resuspended oyster biodeposits. TSS was resuspended during mixing-on of the tidal cycle due to high bottom shear stress. Later in the experiment, TSS was mediated by bottom shear stress and stabilizing effects of microphytobenthos. Throughout the experiment, TSS concentrations increased from ~150 mg l^{-1} during Days 0–15 of the experiment in the R_BD tanks to ~275 mg l^{-1} in the second half of the experiment (Days 15–30). Throughout the experiment, TSS concentrations increased from ~80 mg l^{-1} during Days 0–15 in the R tanks to ~200 mg l^{-1} during the second half of the experiment (Days 21–30).

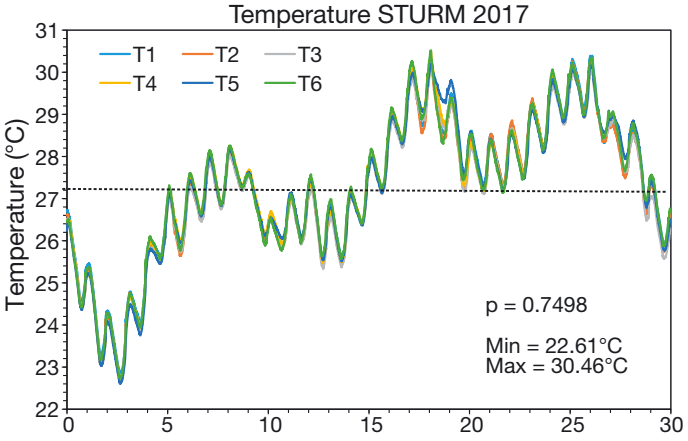

Fig. 2. Temperature in resuspension (R) tanks (T1, T2, T6) and resuspension with daily biodeposit additions (R_BD) tanks (T3, T4, T5) over the experiment, measured in 10 min intervals. Min (Max): minimum (maximum) temperature over the experiment. Mean ± SD temperature in all tanks was 27.22 ± 1.65°C (dashed line), with no statistically significant differences between tanks

Water column chl *a* levels continuously increased from ~5 µg l^{-1} at the beginning of the experiment to ~80 µg l^{-1} at the end of the experiment in the R tanks and increased from ~5 µg l^{-1} at the beginning of the experiment to ~40 µg l^{-1} during Days 10–25 to ~80 µg l^{-1} towards the end of the experiment in the R_BD tanks (Fig. 4a). Chl *a* concentrations were similar between the R and the R_BD tanks (Fig. 4a, p = 0.9085).

Chl *a* did not substantially resuspend and settle in the R_BD tanks, as chl *a* concentrations were the same during the mixing-on and mixing-off phases; however, chl *a* concentrations were significantly reduced in the R tanks during mixing-off compared to R_BD tanks during mixing off (Fig. 4a,d). Phaeophytin concentrations were significantly higher in R_BD tanks than in R tanks, and phaeophytin concentrations differed significantly between the mixing-on and the mixing-off phases as degraded material was resuspended and deposited in R_BD tanks but were similar during the mixing-on and mixing-off phases for R tanks (Fig. 4b,e). The ratio of chl *a* to phaeophytin linearly increased within the first 8 d of the experiment in R tanks (Fig. 4c,f) and was about 4 times higher in R (~2) compared to R_BD tanks (~0.5) from Day 10 to the end of the experiment. It was significantly higher during the mixing-off phase of R_BD systems than during the mixing-on phase, but the ratios were the same during mixing-on and mixing-off for R tanks (Fig. 4f). Finally, during mixing-off, the PC, PN, and PP concentrations were significantly lower in the R tanks than in the R_BD tanks.

PC, PN, and PP concentrations were linearly related to TSS concentrations (Table 4, p < 0.0001), and PC and PN concentrations were significantly enhanced in R_BD tanks (Fig. 3, Table 3). With 8.39 ± 0.88 in R tanks, the C to N ratio was similar as in

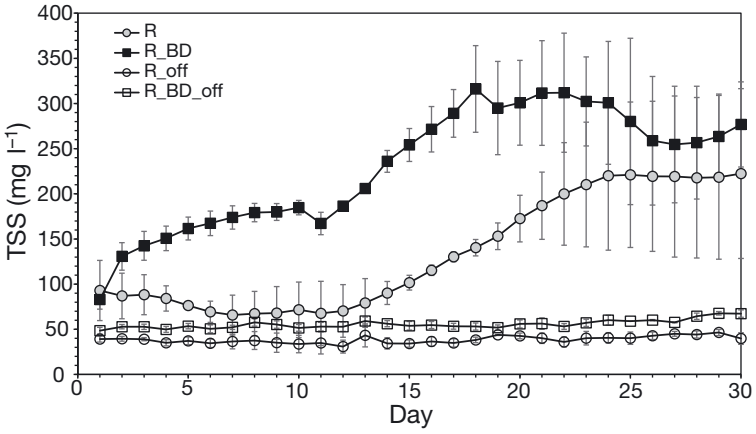

Fig. 3. Total suspended solids (TSS) concentrations (mean ± SD, n = 3 for each system and mixing phase) over time during the mixing-on and mixing-off phases as measured using OBS3 sensors, calibrated with TSS samples. Samples on Day 1 were taken shortly after mixing was started and before biodeposits had been added to the R_BD tanks, which thereafter received daily oyster biodeposit additions over the experiment. Differences between resuspension (R) tanks and R_BD tanks during mixing-on and mixing-off phases were statistically significant ($p \leq 0.05$)

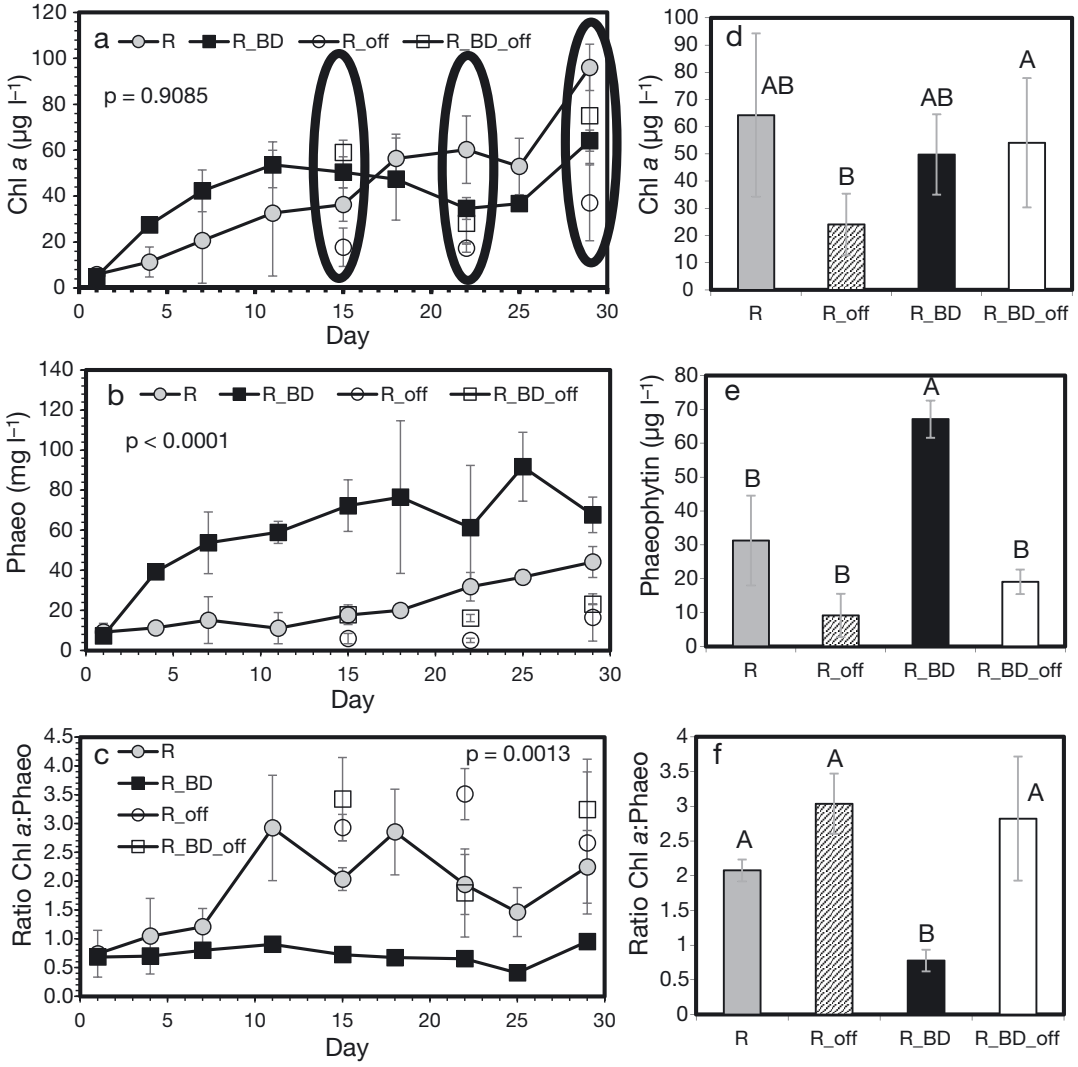

Fig. 4. (a) Chl *a*, (b) phaeophytin (Phaeo), and (c) ratio of chl *a* and phaeophytin concentrations (means ± SD, n = 3 tanks for each system and mixing phase) over time in the resuspension (R) versus the resuspension with daily biodeposit additions (R_BD) tanks during the mixing-on and -off phases. Differences between on phases were statistically significant at $p \leq 0.05$. (d–f) Data from R and R_BD tanks for mixing-on and mixing-off phases averaged over the 3 d indicated by ellipses in panel (a): (d) chl *a*, (e) phaeophytin, and (f) ratio of chl *a* to phaeophytin during mixing-on and mixing-off phases. Different letters indicate statistical differences ($p \leq 0.05$)

R_BD tanks (8.23 ± 0.13; Table 3, p = 0.6214). Much of the PN, PC, and PP settled out during mixing-off phases in all tanks.

While chl *a* concentration was similar between R tanks and R_BD tanks (Fig. 4a, Table 3), significant differences in the phytoplankton community were observed through use of HPLC (Fig. 5) and taxonomic enumerations of phytoplankton biomass (Fig. 6). In addition, the ratio of chl *a*:carbon was significantly higher in R_BD tanks than in R tanks (p = 0.0002; Fig. 6g, Table 3).

Nitrate plus nitrite concentrations (NO_2^- + NO_3^-, p = 0.0433; Fig. 7b, Table 3) and DIN concentrations (p = 0.0395; Fig. 7c, Table 3) were significantly higher in tanks that received biodeposits than in R tanks. TDN (Fig. 7e) and TDP (Fig. 7h) were significantly higher in R_BD tanks than in R tanks over the

Table 4. Linear relationship of total suspended solids (TSS) and particulate carbon (PC), particulate nitrogen (PN), and particulate phosphorus (PP) (all in mg l^{-1}), and linear relationship between PN and PC

Regression	R^2	n	p
PC = 0.0521 × TSS − 0.5739	0.90	69	<0.0001
PN = 0.0071 × TSS − 0.0564	0.87	69	<0.0001
PP = 0.0014 × TSS − 0.0046	0.89	70	<0.0001
PN = 0.1375 × PC + 0.0109	0.99	69	<0.0001

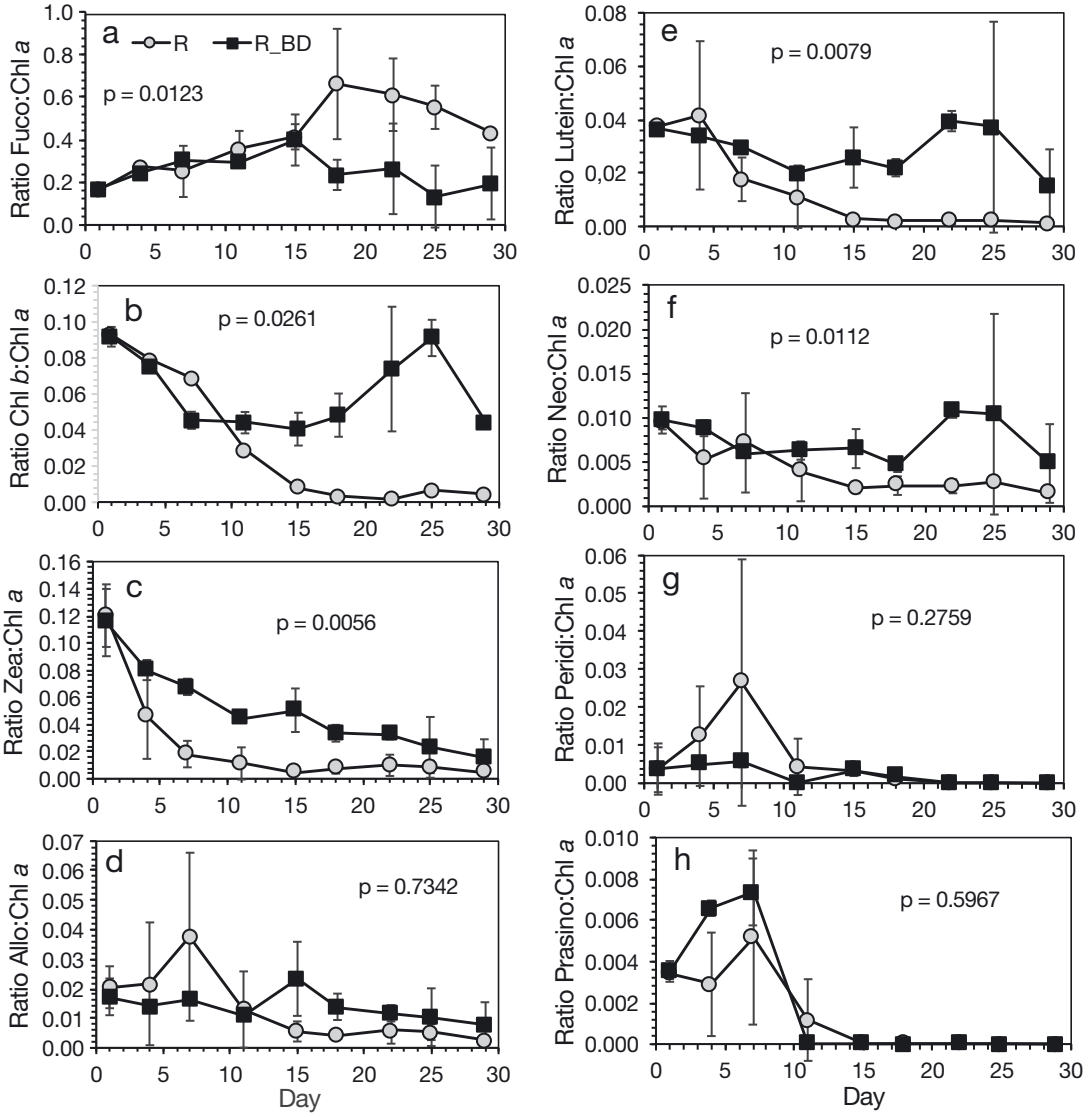

Fig. 5. Ratios of phytoplankton accessory pigments to chl *a* (all measured by HPLC). N = 3 tanks for each system, means ± SD. (a) Fucoxanthin:chl *a*, (b) chl *b*:chl *a*, (c) zeaxanthin:chl *a*, (d) alloxanthin:chl *a*, (e) lutein:chl *a*, (f) neoxanthin:chl *a*, (g) peridinin:chl *a*, (h) prasinoxanthin:chl *a*

second half of the experiment (Day 15 to the end, p = 0.0015 and p = 0.0049, respectively).

Dissolved phosphate (PO_4^{3-}) concentrations (Fig. 7f) decreased in all tanks from ~1.5 µmol l^{-1} at the start of the experiment to ~0.2 µmol l^{-1} on Day 15. After Day 15, it increased again to ~0.3 µmol l^{-1} in the R_BD tanks but remained at ~1 µmol l^{-1} in R systems that experienced a bloom of *Skeletonema costatum* (>2000 µg C l^{-1}). While nutrient concentrations were related to the phytoplankton cell counts in R and R_BD tanks, they did not relate to the chl *a* concentrations. Ammonium (NH_4^+) concentrations were similar between R and R_BD tanks (p = 0.3316; Fig. 7a, Table 3). DOP and DON concentrations (Fig. 7g,d, Table 3) were similar in all tanks. Dissolved silicate concentrations ranged from about 100 to 20 µmol l^{-1} over the experiment, and silicate was at no time limiting, i.e. <5 µmol l^{-1}, in any of the systems (Fig. 7i).

3.3. Light penetration

Light, as measured by a modified Secchi disk, penetrated 25 cm into R_BD tanks during resuspension (Fig. 8a) and 20–50 cm into R tanks during mixing-on. During the mixing-off phases, Secchi depth reached between 30 and 50 cm in R_BD tanks and ~80 cm in tanks that had not received oyster biodeposits

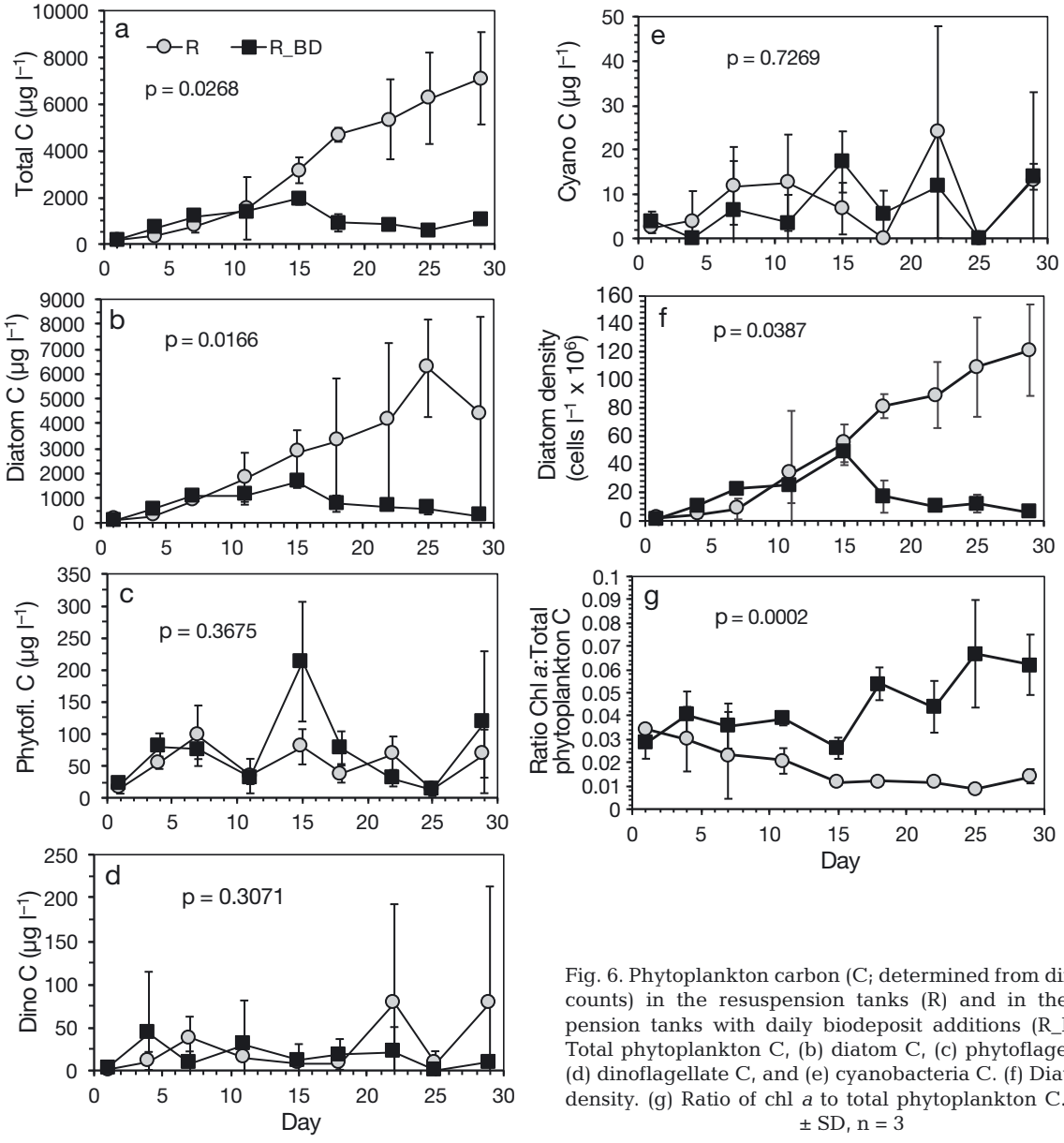

Fig. 6. Phytoplankton carbon (C; determined from direct cell counts) in the resuspension tanks (R) and in the resuspension tanks with daily biodeposit additions (R_BD). (a) Total phytoplankton C, (b) diatom C, (c) phytoflagellate C, (d) dinoflagellate C, and (e) cyanobacteria C. (f) Diatom cell density. (g) Ratio of chl *a* to total phytoplankton C. Means ± SD, n = 3

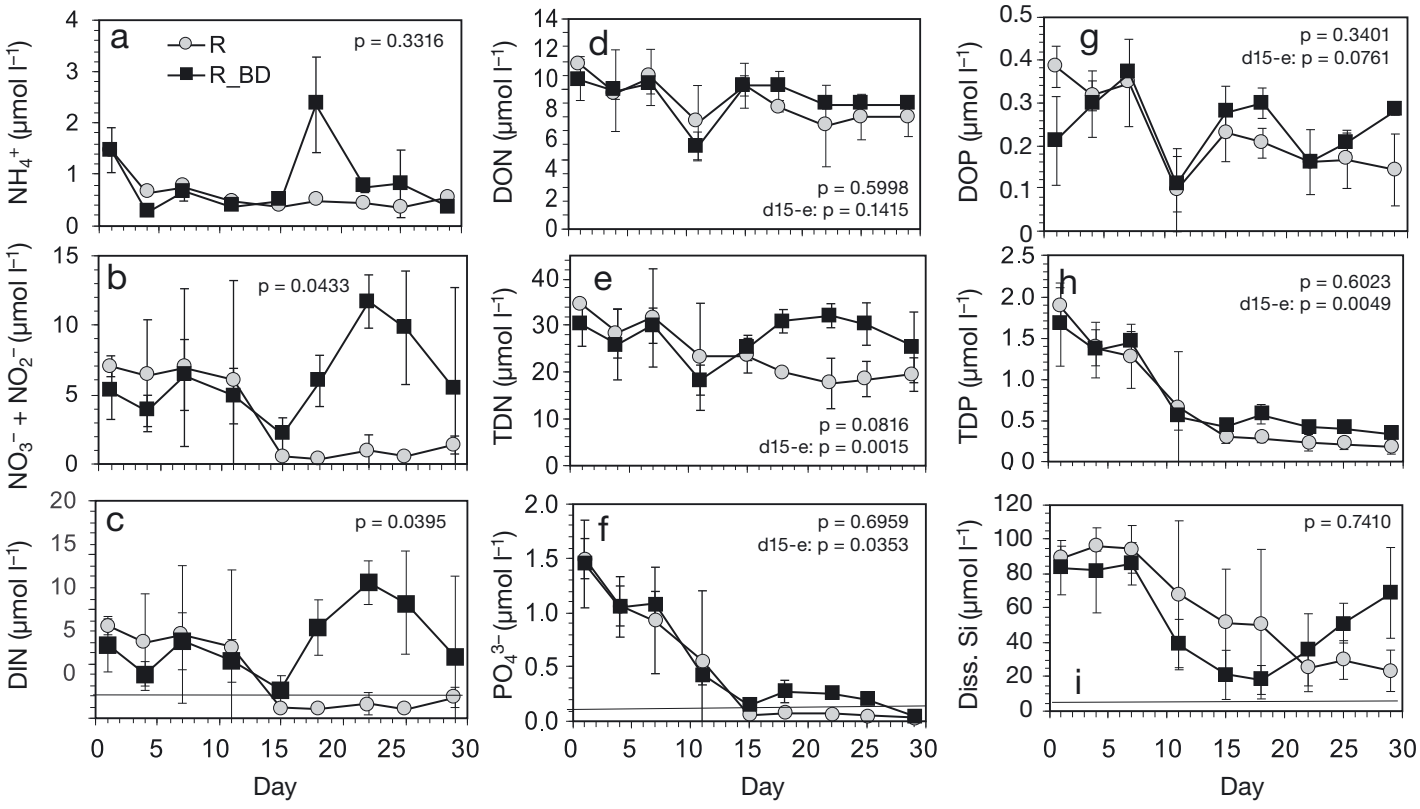

Fig. 7. (a) Ammonium (NH_4^+), (b) nitrate + nitrite (NO_3^- + NO_2^-), (c) dissolved inorganic nitrogen (DIN), (d) dissolved organic nitrogen (DON), (e) total dissolved nitrogen (TDN), (f) phosphate (PO_4^{3-}), (g) dissolved organic phosphorus (DOP), (h) total dissolved phosphorus (TDP), (i) dissolved silica. The horizontal dashed lines in panels c, f, and i indicate thresholds for nutrient limitation for the respective nutrients (see Section 3); d15-e: Day 15 to the end of the experiment. Means ± SD, n = 3

(Fig. 8a). Measured bottom irradiance levels during the resuspension phase were low in R_BD and R tanks due to high turbidities as a result of high TSS concentrations (Fig. 3). Irradiance at the sediment surface during mixing-on was similar in the R (~2.03 ± 1.89 µmol m^{-2} s^{-1}) and in the R_BD systems (0.57 ± 1.4 µmol m^{-2} s^{-1}, p = 0.1126). Geometric mean irradiance in the water column during mixing-on was higher in R tanks with ~16.24 ± 3.11 µmol m^{-2} s^{-1} than in R_BD tanks with 6.43 ± 7.05 µmol m^{-2} s^{-1} (p = 0.0489; Fig. 8b) that had higher TSS concentrations. During the mixing-off phase, significantly more light reached into all tanks than during mixing-on, and, light levels were higher in R tanks than in R_BD tanks during mixing-off (p = 0.0014; Fig. 8b). Significantly more light reached into R tanks than R_BD tanks with mixing-on and -off combined as determined with a Student Newman Keuls test in SAS 8.2 ($p \leq 0.05$).

Microphytobenthos grew on the sediment bottoms of tanks despite high bottom shear stress (~0.36–0.51 Pa during mixing-on phases; Fig. 1c). Light limitation (Fig. 8b) and sediment chl *a* concentrations were similar, with 42.75 ± 3.05 mg m^{-2} in R tanks and 38.77 ± 6.20 mg m^{-2} in R_BD tanks (p = 0.5541). Sediment phaeophytin concentrations with 206.53 ± 17.25 mg m^{-2} in R tanks and 212.44 ± 21.57 mg m^{-2} in R_BD tanks were not significantly different (p = 0.7767).

3.4. Particle settling

Defining an estimate of the bulk settling velocity as the distance from the surface to the turbidity sensor (0.5 m depth) divided by the time to reduce the initial TSS concentration by 50% of the range to its steady state value, bulk settling speeds changed in R_BD tanks over the course of the experiment while they hardly changed in R tanks (Fig. 9). While particles settled slowly on Day 2 (bulk settling speed 0.5 to 0.7 mm s^{-1} in all systems), bulk settling speeds increased continuously to about 2 mm s^{-1} until Day 14 in R_BD tanks, and after Day 15 increased dramatically to 4 to 8 mm s^{-1} in the R_BD tanks over the second half of the experiment. The switch to increased bulk settling speeds coincided with the

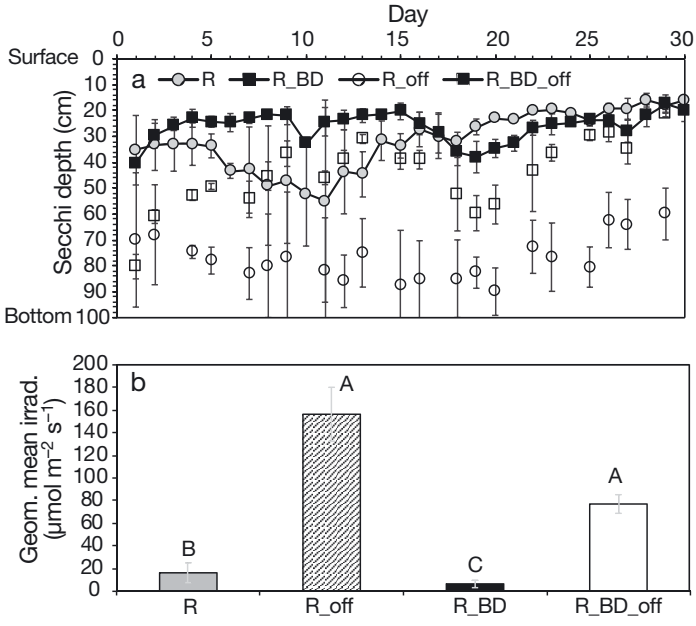

Fig. 8. (a) Mean ± SD Secchi depth measured in resuspension (R) and resuspension with daily biodeposit additions (R_BD) systems during the mixing-on and mixing-off phases over the experiment. (b) Mean ± SD geometric mean irradiance during mixing-on and -off phases; different letters indicate statistical differences ($p \leq 0.05$); n = 3 for each system

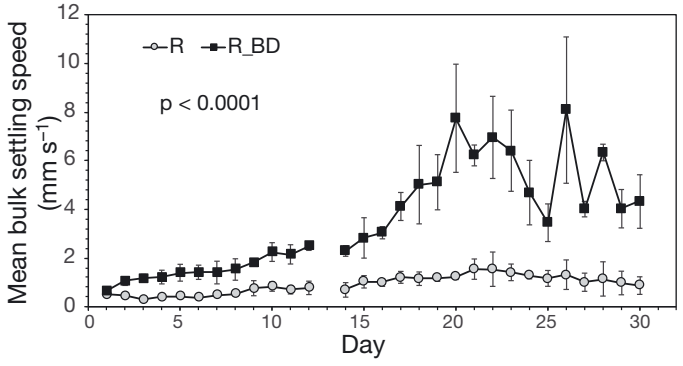

Fig. 9. Mean ± SD bulk settling speeds over time in systems with tidal resuspension (R) and in systems with tidal resuspension and daily additions of oyster biodeposits (R_BD); n = 3 for each system

start of an increase in TSS (Fig. 3), phosphate (Fig. 7f), DIN (Fig. 7c), and nitrate + nitrite (Fig. 7b) concentrations that lasted for the remainder of the experiment (Fig. 7). The ratio of POM:PIM was similar in the R (0.24 ± 0.07) and R_BD tanks (0.23 ± 0.04, p = 0.8908). In addition, this increase in nutrient concentrations overcame nutrient limitation in R_BD systems while the R systems became nutrient limited (DIN: <2 µmol l^{-1}, PO_4^{3-}: <1 µmol l^{-1}, Fig. 7c,f; Fisher et al. 1992, 1999, Poikane et al. 2019).

3.5. Phytoplankton

Diatoms, phytoflagellates, dinoflagellates, chlorophytes, and cyanobacteria were found in the tanks using direct counts (Table 5). While direct counts of dinoflagellate abundances (Fig. 6d) and HPLC (peridinin, Fig. 5g) were similar in all tanks, diatom abundance was significantly higher in R tanks than in R_BD tanks (Fig. 6b,f), indicated by the fucoxanthin signal in the HPLC results (Fig. 5a). *S. costatum* was the dominant diatom in R tanks, and was significantly more abundant there than in R_BD tanks (p = 0.0141; Fig. 10a). In addition, average *S. costatum* chain length was significantly longer in R tanks (11.2 ± 0.2 cells per chain) than in R_BD tanks (9.8 ± 0.6 cells per chain, p = 0.0036; Fig. 10b) as determined from 360 individuals in the R tanks and 190 individuals in the R_BD tanks. The ratio of alloxanthin to chl *a* (indicative of Cryptophyceae) was significantly higher in R_BD tanks in the second half of the experiment (Fig. 5d), and direct counts detected *Cryptomonas* sp. in the tanks.

Chlorophytes were significantly more abundant in R_BD tanks, as the ratio of chl *b* to chl *a* was significantly higher in R_BD tanks than in R tanks (Fig. 5b). Moreover, neoxanthin and lutein (both indicative of Chlorophyceae and Prasinophyceae) were significantly higher in R_BD tanks (Fig. 5f,e), but there were no significant differences in prasinoxanthin (indicating Prasinophyceae) between treatment tanks (Fig. 5h). Thus, chlorophytes were significantly more abundant in biodeposit tanks than in the R tanks.

Direct counts of cyanobacterial abundance were not significantly different (Fig. 6e), although the ratio of zeaxanthin to chl *a*, often used to indicate cyanobacteria (e.g. Van Meerssche & Pinckney 2019) but sometimes used to indicate prochlorophytes, rhodophytes and some Chlorophyceae (Jeffrey & Vesk 1997), was significantly higher in biodeposit tanks (Fig. 5c). It is possible that very small prochlorophytes were in the samples that cannot be counted with the Utermöhl technique used in this study, as picoplankton have to be counted with fluorescence microscopy (MacIsaac & Stockner 1993) or analyzed by flow cytometry (Veldhuis & Kraay 2000).

Total phytoplankton biomass (Fig. 11a), total cell density (Fig. 11g), diatom biomass (Fig. 11b), and phytoflagellate biomass (Fig. 11c) were significantly lower at time zero than during the experiment (Days 2–29) in all treatments, while dinoflagellate biomass was variable (Fig. 11d). Over the course of the exper-

Table 5. Phytoplankton species found in our samples and their cell volumes determined after Smayda (1978) and their carbon constants after Strathmann (1967). Cyano: cyanobacteria; P: phytoflagellate; D: diatom; Dino: dinoflagellate. Also see Fig. 13

Taxon	Type	Carbon constant	Cell volume (μm^3)
Size 1			
Blue-green algae filament	Cyano	2.42	3.5
Salpingoeca sp.	P	11.19	29.9
Cryptomonas <10 µm	P	11.78	32.2
Scenedesmus quadricauda	D	11.78	32.2
Unid. microphytobenthos <10 µm	P	20.81	71.6
Pennate diatom <10 µm	D	23.74	86.2
Unident. diatom	D	24.4	89.6
Unident. centric diatom <10 µm	D	25.05	93
Cyclotella <10 µm	D	33.25	138.6
Cylindrotheca closterium	D	33.86	142.2
Prorocentrum minimum	Dino	35.18	150
Neidium sp.	D	48.31	234.4
Skeletonema costatum	D	48.99	239.1
Size 2			
Chaetoceros sp.	D	52.82	265.8
Chaetoceros subtilis	D	60.21	319.6
Leptocylindrus minimus	D	64.64	353.2
Pyramimonas sp.	P	69.26	389.2
Gymnodinium 10–20 µm	Dino	74.2	428.9
Cryptomonas >10 µm	P	75.73	441.4
Gyrodinium 10–20 µm	Dino	90.01	562.9
Leptocylindrus denicus	D	97.1	626.3
Pennate diatom 10–30 µm	D	98.37	637.8
Cylindrotheca closterium >40 µm	D	105.02	699.3
Unid. microphytobenthos >10	P	126	903.7
Unident. centric diatom 10–30 µm	D	143.01	1080
Navicula sp.	D	143.48	1085
Thalassionema nitzschoides	D	163.85	1307.9
Coscinodiscus	D	230.31	2112
Pennate diatom 31–60 µm	D	233.355	2151.4
Neidium sp. Large	D	247.07	2331.5
Amphidinium sp.	Dino	315.24	3285.3
Prorocentrum sp.	Dino	364.46	4029.6
Gymnodinium splendens	Dino	489.4	6101.6
Size 3			
Gymnodinium 21–50 µm	Dino	601.18	8150.6
Unident. centric diatom 31–60 µm	D	664.94	9393
Pleurosigma sp.	D	682.39	9741.8
Amphipora alata	D	941.98	15335.7
Gymnodinium 51–70 µm	Dino	2302.4	53952.2
Unident. centric diatom >60 µm	D	2342.84	55290.7

iment, biomass shifted towards a diatom-dominated phytoplankton community, especially in R tanks where the percentage of phytoplankton community composed of diatoms increased by 31% (Fig. 12). In addition, over the second half of the experiment, most diatoms (84.4%) in R tanks were *S. costatum* by cell density, contrasted with only 6.8% of diatoms in biodeposit tanks.

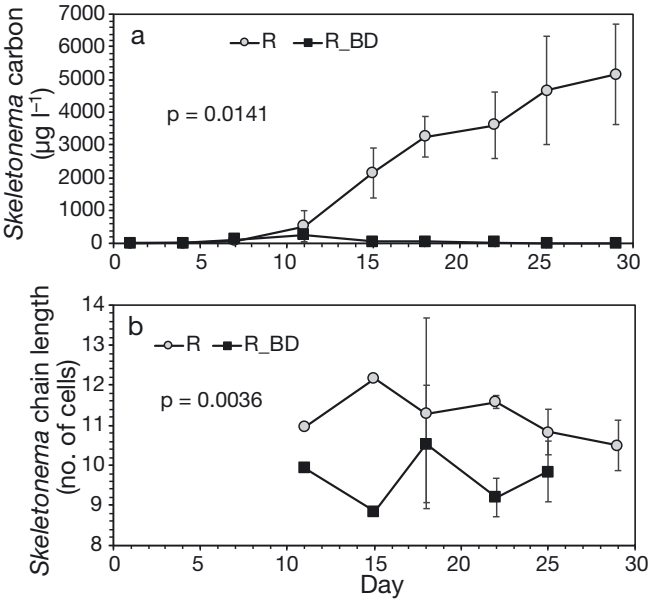

Fig. 10. (a) Mean ± SD *Skeletonema costatum* carbon concentrations in resuspension (R) tanks and in resuspension with daily biodeposit additions (R_BD) tanks over the experiment, n = 3. (b) Mean ± SD *S. costatum* chain length (no. of cells) in R and in R_BD tanks over the experiment. Average *S. costatum* chain length was 11.2 ± 0.2 cells in R tanks and 9.8 ± 0.6 cells in R_BD tanks

Over the course of the experiment, the abundance of small phytoplankton cells (cell volume of 3–240 μm^3; Table 5) increased continuously in R tanks, and the biomass of small cells was significantly higher with 2704.5 ± 2034.3 µg C l^{-1} than the biomass of larger cells (cell volume of 241–65 300 μm^3; Table 5) with 788.3 ± 474.6 µg C l^{-1} ($p = 0.0319$; Fig. 13c). In contrast, with a biomass of 557.0 ± 422.2 µg C l^{-1}, small cells did not dominate the phytoplankton community in the biodeposit tanks where large cells had a biomass of 359.9 ± 138.4 µg C l^{-1} ($p = 0.2450$; Fig. 13d). In the second half of the experiment, 85.6 and 5.7% of the small phytoplankton (cell volume of 3–240 μm^3; Table 5) were *S. costatum* in R tanks and R_BD tanks, respectively.

Some patterns of species abundance, in addition to *S. costatum*, emerged from direct phytoplankton counts. Small individuals of the diatom *Cyclotella* sp. (smaller than 10 µm, size 1; Table 5) were found in R_BD tanks throughout the experiment. *Cyclotella* sp. was only found during the first half of the experiment in R tanks and was completely absent during the second half of the experiment. Another small diatom, *Cylindrotheca closterium* (size 1; Table 5), was found in all tanks throughout the experiment. However, *C. closterium* larger than 40 µm (size 2; Table 5) was abundant in the R tanks during the sec-

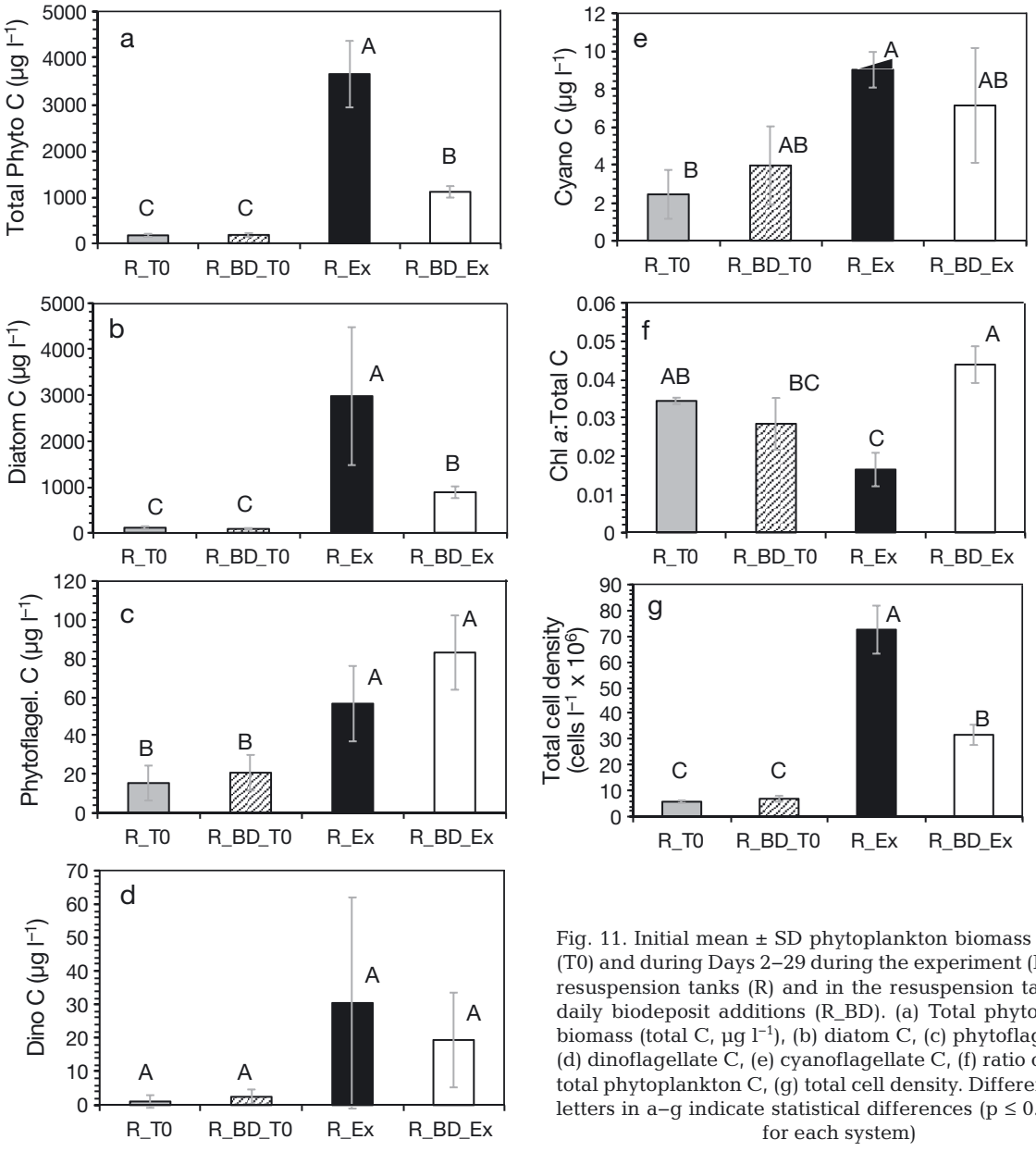

Fig. 11. Initial mean ± SD phytoplankton biomass at time 0 (T0) and during Days 2–29 during the experiment (Ex) in the resuspension tanks (R) and in the resuspension tanks with daily biodeposit additions (R_BD). (a) Total phytoplankton biomass (total C, µg l^{-1}), (b) diatom C, (c) phytoflagellate C, (d) dinoflagellate C, (e) cyanoflagellate C, (f) ratio of chl *a* to total phytoplankton C, (g) total cell density. Different capital letters in a–g indicate statistical differences ($p \leq 0.05$, n = 3 for each system)

ond half of the experiment, and only appeared occasionally in R_BD tanks. The dinoflagellate *Gymnodinium* sp. (10–20 µm, size 2; Table 5) was abundant in the R_BD tanks during the second half of the experiment while it was mostly abundant in the R tanks during the first half of the experiment. The phytoflagellates *Cryptomonas* sp. and *Pyramimonas* sp. (size 2; Table 5) were abundant in all tanks during the first part of the experiment and disappeared entirely during the second half of the experiment. While the diatom *Thalassionema nitzschoides* (size 2; Table 5) was more abundant in the first half of the experiment in the R_BD tanks, it was mostly more abundant in the second half of the experiment in the R tanks. The diatom *Chaetoceros* sp. (size 2; Table 5) was present in the second half of the experiment in the R tanks and only very occasionally detected in R_BD tanks. *Scenedesmus quadricauda* was rare and was encountered only once in a single R tank.

3.6. Macrofauna and mesozooplankton

No macrofauna was observed in any tanks at the end of the experiment, but mesozooplankton was abundant in biodeposit tanks. Dominant mesozoo-

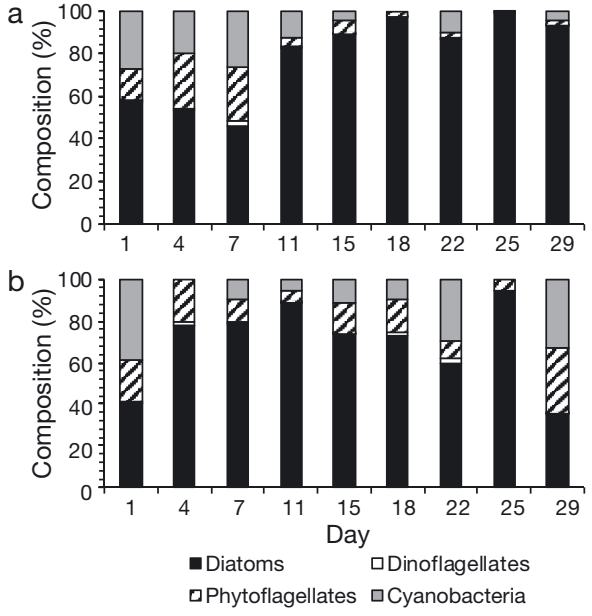

Fig. 12. Percent composition by cell density of diatoms, phytoflagellates, dinoflagellates, and cyanobacteria over the experiment in (a) resuspension tanks (R) and (b) in resuspension tanks with daily biodeposit additions (R_BD). Day 1 is T0

plankton taxa were adult *Acartia tonsa* copepods (Fig. 14d), copepodites (Fig. 14e), copepod nauplii (Fig. 14c), and polychaete larvae (Fig. 14b, Table 3). It took nearly 1 wk for adult copepods and 10 d for polychaete larvae to be detected (Fig. 14d,b). Pumps likely destroyed the adult mesozooplankton stages (Adey & Loveland 1998) during the initial raw water fill of the tanks at the start of the experiment. The R_BD tanks contained 52.32 ± 27.17 adult *A. tonsa* l^{-1} throughout the experiment ($p = 0.0018$; Fig. 14d, Table 3), while R tanks contained 4.99 ± 3.45 adult *A. tonsa* l^{-1}. On days during the heat wave (Days 13–17), *A. tonsa* abundance in the water column decreased to about 42 to 47 ind. l^{-1} in R_BD systems (Fig. 14d) when copepods potentially migrated towards the bottom of the tank; however, they increased again on Day 21. Polychaete larvae continuously increased in all systems up to 80–99 ind. l^{-1} in both systems at the end of the experiment, and polychaete concentrations were not significantly different between tanks ($p = 0.3559$; Fig. 14b). Polychaete larvae were grouped by size (large = ~0.536 mm; small = ~0.152 mm) for carbon determinations. Occasionally, veliger larvae, harpacticoid copepods, flatworms, nematodes, cyclopoid copepods, and other calanoid copepods were found, but abundances were similar between treatments (Table 3). In addition, rotifers (>63 µm) were caught in our zooplankton net. The mesozooplankton community was positively correlated with phytoplankton biomass (from counts, converted to carbon) in R tanks (Fig. 14f) but not in R_BD tanks (Fig. 14g).

4. DISCUSSION

4.1. Suspended solids, water clarity, and biogeochemistry

TSS concentrations increased due to added resuspended oyster biodeposits (e.g. Hildreth 1980), and particle settling rates likely increased because of particles adhering to each other. While the effect of suspended sediment concentration on particle size is not understood (Berhane et al. 1997, Walker et al. 2005), both the mass and size of particles is dependent on the energy dissipation rate. The floc settling rate is influenced by floc composition and the ratio of POM:PIM, which was similar in R and R_BD tanks, shape, porosity, and water content (Droppo et al. 1997). Measured particle sinking velocities of ~1–8 mm s^{-1} in oyster biodeposit tanks (Fig. 9) were consistent with biodeposit settling rates of 0.19–16.25 mm s^{-1} for zebra mussels *Dreissena polymorpha* (McLean et al. 2018), 3–18 mm s^{-1} for *Mytilus edulis* biodeposits (Callier et al. 2006), 1–18 mm s^{-1} for *M. edulis* biodeposits (Chamberlain et al. 2001), and 1–45 mm s^{-1} for green-lipped mussel *Perna canaliculus* biodeposits (Giles & Pilditch 2004).

TSS concentrations in the second half of the experiment were more variable, probably due to microphytobenthos formation, stabilizing some tanks more than others (Yallop et al. 1994, Widdows & Brinsley 2002). Despite some variability in TSS concentration, clear differences in ecological responses were detectable in R and R_BD tanks (e.g. see phytoplankton in Section 3.5 and zooplankton in Section 3.6).

Oyster biodeposit additions decreased water clarity and light availability and increased water column nitrate + nitrite concentrations. Nitrate + nitrite and phosphate concentrations during the second part of the experiment were significantly higher in tanks with biodeposits. Biogeochemical sediment nutrient and gas fluxes, also measured in this experiment, were similar between the R and R_BD tanks (unpubl. data).

4.2. Algal biomass and composition

Tanks with sediment resuspension had increased chl *a* concentrations (Porter et al. 2010) beyond the management threshold of 40 µg chl *a* l^{-1} (Sutula et al.

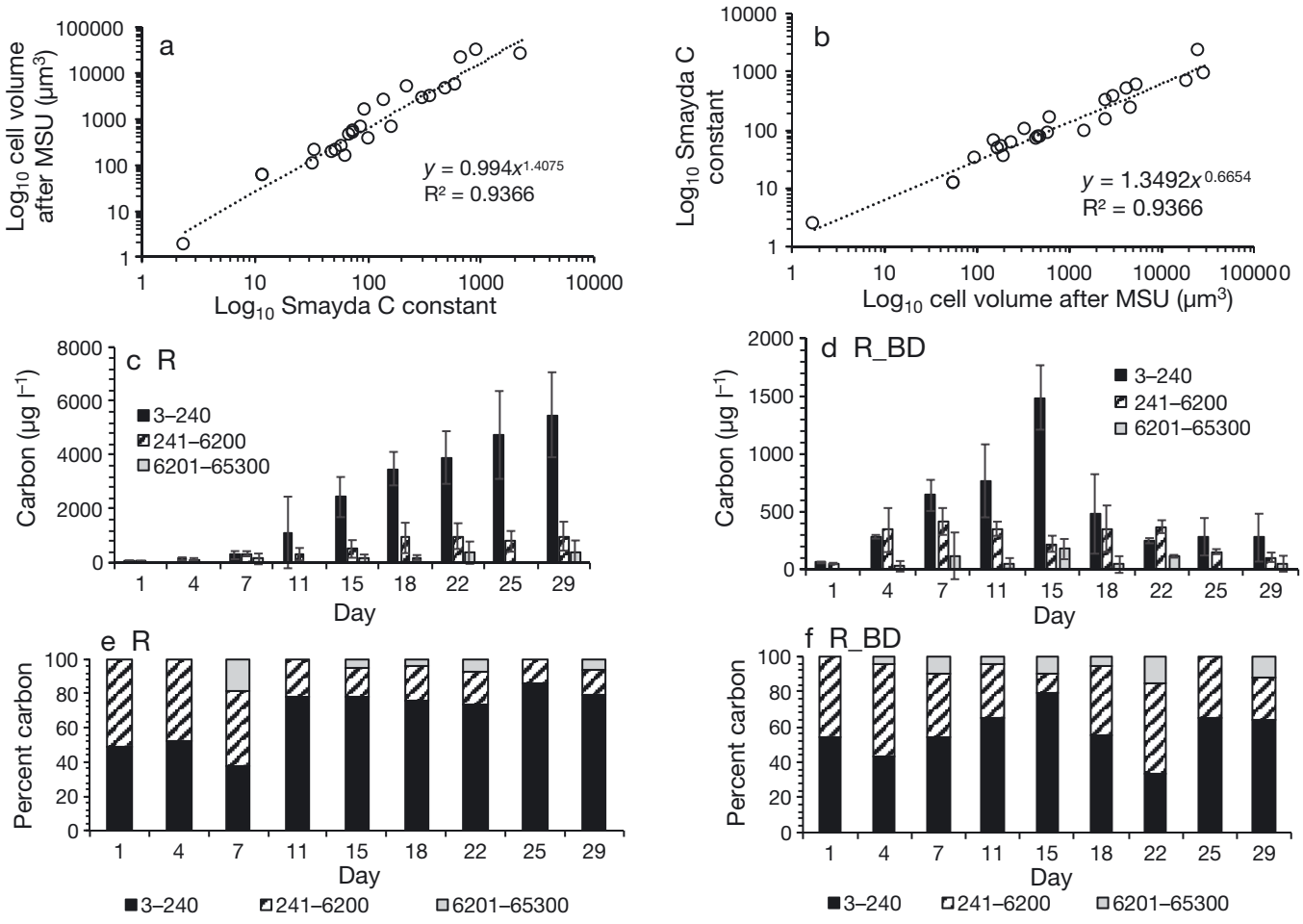

Fig. 13. Relationship of (a) cell volume (µm^3) and (b) carbon constant determined after Strathmann (1967; MSU: Morgan State University) and Smayda (1978). Mean ± SD carbon content in 3 different phytoplankton cell volume ranges (µm^3) in the (c) resuspension (R) tanks and (d) resuspension with daily biodeposit additions (R_BR) tanks, respectively; n = 3 for each system. Percent contribution of each size fraction to the phytoplankton biomass in the (e) R and (f) R_BD tanks

2017). Such sediment resuspension may enhance sediment nutrient release (Morin & Morse 1999) or conversely dampen the effect of nutrient inputs on the phytoplankton community (Kang et al. 2013). To examine the role of resuspended biodeposits and associated nutrients on phytoplankton abundance with high bottom shear and realistic water column turbulence, our initial hypothesis was that biodeposit additions and resuspension enhances nutrient concentrations (Porter et al. 2018a). Increased chl *a* concentrations (Browning et al. 2019, Gerhard et al. 2019), and community structure (Medina-Gómez et al. 2019, Villamaña et al. 2019) are a likely result.

The non-significant differences in chl *a* concentration between treatments (Fig. 4a) were inconsistent with significantly higher direct counts of phytoplankton biomass in R tanks relative to R_BD tanks. These observations refute our original hypothesis. Phytoplankton direct cell counts and HPLC pigments show significant effects of tidal sediment and biodeposit resuspension on the phytoplankton abundance and community structure. The effects of differential mixing on phytoplankton abundance and community structure (Iversen et al. 2010, Fouilland et al. 2016) were controlled for in this experiment, ensuring similar turbulence intensity, volume-weighted energy dissipation rate, and bottom shear stress. Biodeposition may alleviate phytoplankton growth limitation during periods of N limitation (Cranford et al. 2007). While in R_BD tanks nutrients were never limiting, nutrient limitation is inferred in R tanks after Week 15 (Fig. 7c,f) if published nutrient limitation thresholds for dissolved silicate of <5 µmol l^{-1}, DIN <2 µmol l^{-1} (Mediterranean threshold, Poikane et al. 2019), and phosphate <0.1 µmol l^{-1} (Fisher et al. 1992, 1999, T. Fisher pers. comm.) are applied.

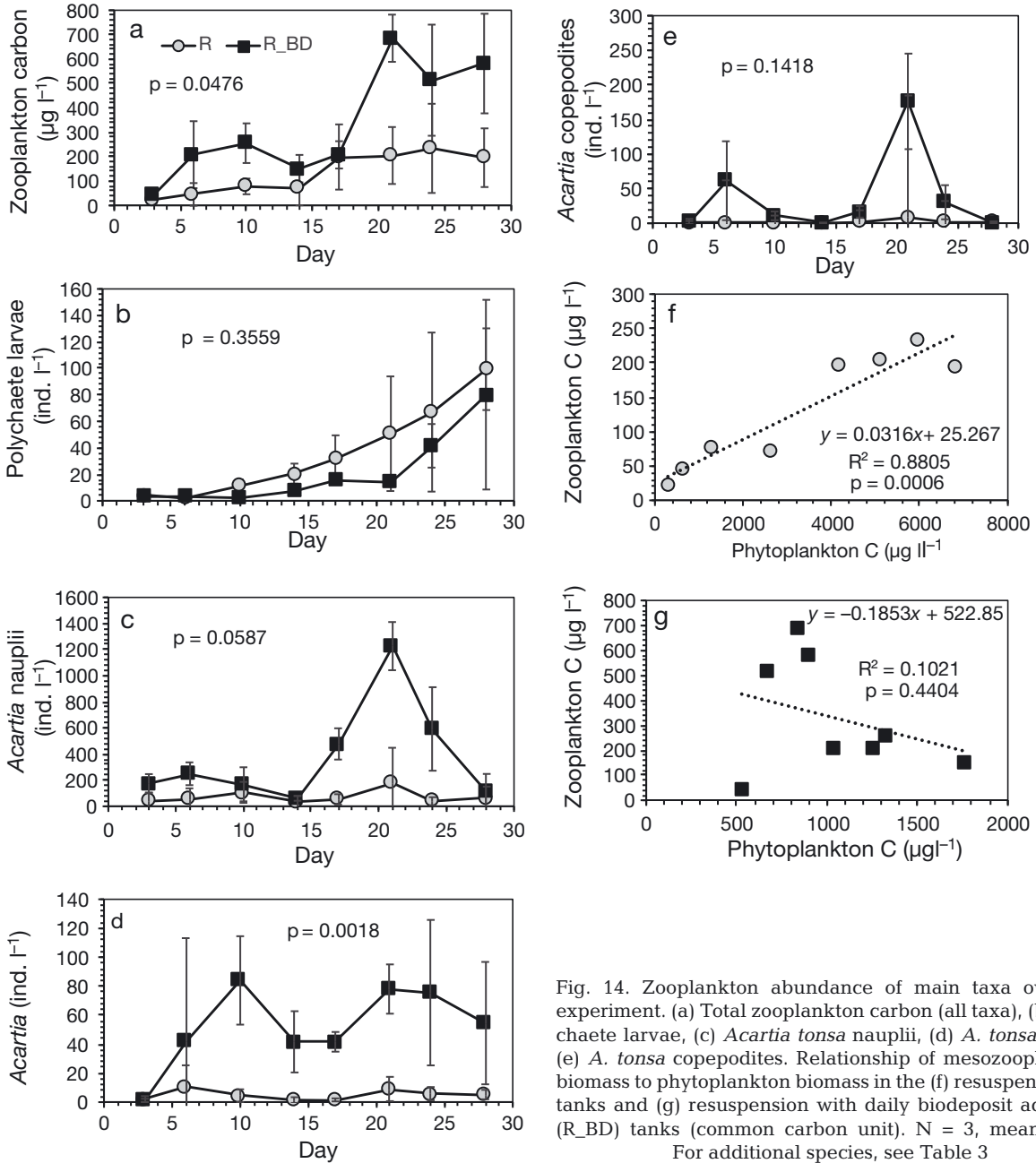

Fig. 14. Zooplankton abundance of main taxa over the experiment. (a) Total zooplankton carbon (all taxa), (b) polychaete larvae, (c) *Acartia tonsa* nauplii, (d) *A. tonsa* adults, (e) *A. tonsa* copepodites. Relationship of mesozooplankton biomass to phytoplankton biomass in the (f) resuspension (R) tanks and (g) resuspension with daily biodeposit additions (R_BD) tanks (common carbon unit). N = 3, mean ± SD. For additional species, see Table 3

Skeletonema costatum blooms after Day 15 significantly reduced nitrate + nitrite and phosphate concentrations in R tanks and potentially suppressed cryptophytes and cyanobacteria, as diatoms can rapidly take up and store nitrate, and outcompete cryptophytes and cyanobacteria (Lomas & Glibert 2000, Clark et al. 2002, Sarthou et al. 2005, Kamp et al. 2015). In contrast, chlorophytes became significantly more abundant in biodeposit tanks after Day 15 where no nutrient limitation was experienced.

The R_BD tanks with fewer *S. costatum* and shorter chain lengths had significantly higher nitrate + nitrite levels than R tanks, with both higher nutrient levels and increasing temperature associated with smaller chain length in phytoplankton (Takabayashi et al. 2006). Although chain lengths remained significantly longer in R tanks, chain length decreases in the second half of the experiment coincided with increased temperatures and decreased nutrient concentrations. Moreover, R_BD tanks with significantly shorter chain length had significantly higher abundances of *Acartia tonsa*. *S. marinoi* (1 of 6 subspecies of *S. costatum*; Bergkvist et al. 2012) changes morphology to a single-celled or shorter-chain phenotype when

exposed to *A. tonsa* (Bergkvist et al. 2012). Copepod chemical cues have been observed to trigger chain fragmentation in *S. marinoi* (Bergkvist et al. 2012), and the significantly higher abundance of *A. tonsa* in biodeposit tanks may have provided chemical cues for chain splitting so that chain length was significantly shorter in these tanks than in R tanks. Copepodamide chemical cues, released by marine zooplankton, also triggered defenses such as chain length shortening in a study by Grebner et al. (2019). Grazing activity increased chain length (Martin 1970, Deason 1980, O'Connors et al. 1980); however, Bjærke et al. (2015) suggested this could be due to the induced splitting of chains. *Skeletonema* chain length decreased with increasing abundance of mesozooplankton (Turner et al. 1983), which is also supported in our study. Other studies found that certain algae (Scenedesmaceae) prevent predation by increasing their size (via added chain length) or develop armor spines (Hessen & Van Donk 1993) when exposed to copepods (Bjærke et al. 2015); however, *S. costatum* has no spines as defenses.

Observations of chain length increases with experimental silicate limitation (Fouilland et al. 2016) may arise because diatom cells stop their cellular cycle in the G2 phase at their maximum size (Martin-Jézéquel et al. 2000). However, the absence of silicate limitation in our experiment (Fig. 7i) is not consistent with longer chain lengths. Since light absorption is higher for smaller cell fragments than for larger cell fragments (Agusti 1991, Finkel & Irwin 2000), less light in biodeposit tanks would have allowed the smaller *S. costatum* fragments in these tanks to absorb more light. Moreover, the ratio of chl *a*:carbon was significantly higher in R_BD tanks that were more light limited than R tanks ($p = 0.0002$; Fig. 6g), which suggests an adaptation to the low light regime in R_BD tanks by increasing the chl *a* content per cell in the phytoplankton (Buchanan et al. 2005, Porter et al. 2018a). Phytoplankton acclimate to light limitation by changes in pigment concentration to maximize photosynthetic rate (Finkel et al. 2004). Following the phytoplankton size analysis above, there was no shift to smaller phytoplankton in the R_BD tanks ($p = 0.2450$) to potentially explain the shift to a higher chl *a*:carbon ratio in the R_BD tanks.

Oyster biodeposit resuspension affects ecosystem components such as the mesozooplankton community, with increased *A. tonsa* biomass in R_BD tanks relative to R tanks. While the mesozooplankton community was positively correlated with phytoplankton biomass in R tanks (Fig. 13f), zooplankton biomass was low in R tanks, considering that more than a third of carbon transitioned into phytoplankton biomass but subsequently did not translate into zooplankton biomass. Zooplankton grazing of phytoplankton biomass appeared minimal in R tanks with a large bloom of long-chain *S. costatum*. The mesozooplankton community was not correlated with phytoplankton biomass in R_BD tanks (Fig. 14g), and mesozooplankton abundance was higher than expected from phytoplankton biomass.

Biodeposit tanks had a carbon deficiency of 2.54 g compared to R tanks. Phytoplankton carbon in R_BD was 2.54 g lower relative to R tanks. Estimates suggested that mesozooplankton may consume 5–15% of primary production (Carlson 1978, Behrenfeld & Falkowski 1997, Calbet 2001, Anderson et al. 2019). Assuming a 10% trophic transfer to higher-level predators (mesozooplankton), 1.11 g phytoplankton carbon would be converted to 0.111 g mesozooplankton biomass in biodeposit tanks. The same conversion of phytoplankton to mesozooplankton in the R tanks converts 3.65 g of phytoplankton carbon to 0.365 g of mesozooplankton carbon. The difference in phytoplankton to mesozooplankton carbon weight conversions between the treatments shows that biodeposit tanks had only 30% of the biomass conversions (0.111 g) that non-biodeposit tanks (0.365 g) had, despite greatly enhanced zooplankton populations. R tanks had 0.1314 ± 0.037 g carbon zooplankton per tank and thus R_BD tanks were expected to have 0.385 g carbon per tank, which was calculated by adding actual zooplankton carbon, 0.1314 g + established carbon deficiency of biodeposit tanks, 0.254 g; this estimate was similar to observed values (0.3193 ± 0.044 g carbon per tank).

In biodeposit tanks, the 'missing' phytoplankton must have been converted to zooplankton, although potential grazing effects of the microzooplankton community are not included in the analysis. The resuspension of protists may alter the microbial food web (Shimeta et al. 2003), all of which may have selectively affected microzooplankton grazing in tanks. However, decreased microzooplankton abundance has been associated with resuspension (Lawrence et al. 2004). While increased DOC concentrations can yield increased heterotrophic picoplankton concentrations (La Rosa et al. 2002), our DOC concentrations were similar between R and R_BD tanks ($p = 0.6628$), suggesting an expectation of similar heterotrophic picoplankton concentrations between treatments. Olson et al. (2006) also suggested higher abundance of smaller phytoplankton at times of intense mesozooplankton grazing, and increased chlorophyte abundance was detected in

R_BD tanks with intense mesozooplankton grazing, consistent with these observations. However, phytoplankton size analysis revealed that R tanks shifted to smaller (cell volume 3–240 µm^3, including *S. costatum*) phytoplankton species over the experiment ($p = 0.0319$), while biodeposit tanks had no such shift ($p = 0.2450$), refuting this idea. In this experiment, nutrients decreased more in the R than in the R_BD tanks and became limiting in R tanks. The presence of smaller plankton sizes in R tanks (mostly *S. costatum*) is consistent with the available nutrients, because smaller size allows plankton to better compete for nutrients (Riegman et al. 1993).

The low presence of grazing of the long chains of the *S. costatum* bloom in the R tanks is unusual, as copepods generally feed more on longer chains (Bjærke et al. 2015). *S. costatum* took up nitrate + nitrite in R tanks, and more than a third of carbon was partitioned in the phytoplankton in the R tanks, without conversion to mesozooplankton. In R_BD tanks, much of the carbon remained in added biodeposit particulate carbon and was transformed into zooplankton tissue. A lower carbon content of TSS resulted in poor food quality and low grazing rates by zooplankton despite abundance and quality of diatom-dominated algal food in a study by Wood et al. (2016). Food quality on a mass basis (e.g. POM:PIM ratio, C:N ratio) was poor in all tanks due to sediment resuspension.

Multiple studies have shown that *S. costatum* negatively affects copepods. *S. costatum* releases unsaturated C_7 and C_8 aldehydes that may affect the egg hatching success of copepods (d'Ippolito et al. 2002, Pohnert et al. 2002, Pohnert 2005) as found in experiments with diatom cultures, and *S. costatum* and other diatoms release aldehydes that arrest copepod embryo development (Miralto et al. 1999), either of which may have affected the copepod population in R tanks. *S. costatum* can have adverse effects on copepod reproduction, evidenced by the findings of Budge & Parrish (1999) and Pohnert (2005) that 65% of the hatched nauplii of *Calanus helgolandicus* had deformed limbs after feeding on *S. costatum*. *S. costatum* reduces both fecundity and egg hatching success in *Acartia clausi* and causes reduced fecundity but not a reduction in hatching success in *Temora stylifera* (Ban et al. 1997). Jónasdóttir et al. (1998) suggested the potential for phytoplankton toxicity. Perhaps in R tanks the abundant *S. costatum* with long chains negatively affected copepod reproductive success; this would help to explain the lower abundance of copepod nauplii in R than in R_BD tanks during the second half of the experiment. Recent investigations revealed that phytoplankton exhibit defense mechanisms that negatively affect zooplankton (Pančić & Kiørboe 2018).

The >40 µm diatom species with defenses such as spines (Van Donk et al. 2011) included *Chaetocerus subtilis*, *Chaetocerus* sp., and *Cylindrotheca closterium* (= *Nitzschia closterium*) predominantly found in R tanks, with small *C. closterium* present in R_BD tanks. *Scenedesmus quadricauda* was observed only once in this study, in an R tank. Cyanobacteria were observed in both treatments. *C. closterium,* an epizoic diatom species, can proliferate on the surface of copepods (Gárate-Lizárraga & Esqueda-Escárcega 2016). Cyanobacteria likely have poor nutritional quality for zooplankton due to inadequate fatty acid composition (Ahlgren et al. 1992), production of non-ribosomal peptides, e.g. nodularin and spumigin (Mazur-Marzec et al. 2016), and low manageability of the filaments (Gliwicz & Siedlar 1980). Filamentous cyanobacteria have a negative effect on copepod egg production despite high concentrations of non-cyanobacterial food and alter the transfer of the essential micronutrient thiamin (i.e. vitamin B_1) to copepods (Fridolfsson et al. 2018). While cyanobacteria abundance was significantly higher in R_BD tanks ($p = 0.0056$) than R tanks when measured as the ratio of zeaxanthin:chl *a* using HPLC (cyanobacteria abundance was similar using direct counts, $p = 0.7260$), *A. tonsa* was abundant in the R_BD tanks, and we found no negative effects of cyanobacteria on *A. tonsa*.

Less abundant and shorter-chained *S. costatum* were found in biodeposit tanks, suggesting the potential for diatom settling. Longer *S. costatum* chains of live and unstressed (Smayda 1974, Waite et al. 1997) cells have greater buoyancy, whereas shorter chains settle more easily (Smayda & Boleyn 1966). Although the shorter-chained *S. costatum* may have settled out in R_BD tanks contributing to lower *S. costatum* abundance in these tanks, mixing should have countered this effect. *S. costatum* aggregates may have formed during resuspension, promoting faster sinking (Ziervogel & Forster 2005), although energy dissipation rate was similar in all systems. Chl *a* concentrations between mixing-on and mixing-off were not significantly different, suggesting a lack of settling of *S. costatum* in the R_BD tanks.

Although chl *a* measurements are typically used to indicate phytoplankton biomass, using chl *a* alone as an indicator of phytoplankton biomass may be misleading. In this experiment, chl *a* abundance did not differ among treatments, whereas significant differences were detected in phytoplankton biomass

based on the count data and HPLC analysis. As suggested by Van Meerssche & Pinckney (2019), chl *a* measurements should be supplemented with an additional measure of phytoplankton biomass. The significantly higher chl *a*:carbon ratio in biodeposit tanks than in R tanks suggests a low light adaptation of the phytoplankton in R_BD tanks (Buchanan et al. 2005, Porter et al. 2018a).

4.3. Temporal and experimental considerations

In this study, as in Porter et al. (2018a), multiple system effects had a lag time and became apparent only in the second half of the experiment, and phytoplankton acclimated their physiology (and internal stoichiometry) to novel nutrient and light conditions (e.g. Wirtz & Pahlow 2010). Ecosystems are complex with positive and negative feedback loops, high connectivity, non-linear changes, and delays between cause and effect (Scholes & Kruger 2011). The response time for phytoplankton and zooplankton populations to increase after biodeposit addition is affected by the longevity and physiology of the organisms (Harley et al. 2017), transformation and fate of biodeposits, and by the phytoplankton–copepod feedback loops. Episodic meteorological and nutrient-load events can drive coastal planktonic ecosystem dynamics, and Guadayol et al. (2009) observed that nutrient enrichments resulted in increased chl *a* concentrations 1 wk after addition. Longer phytoplankton time lags have been observed, such as 2 wk following resuspension in the German Bight (Su et al. 2015), similar to the time lag in this research.

Short-duration experiments will not necessarily include all of the direct and indirect interactions of nutrient, phytoplankton, and mesozooplankton dynamics. Indirect effects have often been identified by accident when experiments produced unanticipated results (Wootton 2002). In the present case, R tanks were light limited and any regenerated nitrate + nitrite through sediment resuspension was taken up by a bloom of *S. costatum*. While phytoplankton carbon was transferred to *A. tonsa* in the biodeposit treatment with less abundant and shorter-chained *S. costatum* than observed in R tanks, phytoplankton carbon transferred to the mesozooplankton community in R tanks potentially had negative effects on copepod reproduction. Copepods, preying on microzooplankton, allow an increase in phytoplankton in a trophic cascade (Stibor et al. 2004, Vadstein et al. 2004, Armengol et al. 2017). However, in R_BD tanks, the abundant *A. tonsa* decreased phytoplankton abundance and did not release phytoplankton from grazing pressure.

Field observations of the consequences of resuspended sediments and biodeposits are difficult to track (Testa et al. 2015), and typical experimental ecosystem experiments with low bottom shear stress do not support resuspension (Doering et al. 1986, Porter et al. 2010). Although the STURM facility (Porter et al. 2018b) allows high bottom shear stress and realistic water column turbulence levels for benthic–pelagic coupling experiments (Porter et al. 2010, 2013, 2018a), oysters were not directly included in this experiment, as the primary focus was on biodeposits. Bivalve filtration of phytoplankton (Cloern 1982, Cohen et al. 1984, Porter et al. 2004a) would have resulted in competition between zooplankton and oysters for algae. The size distribution of phytoplankton might shift towards smaller species (Souchu et al. 2001, Cranford et al. 2007, Jiang et al. 2019) because oysters efficiently filter phytoplankton larger than 3 µm in size (Haven & Morales-Alamo 1970). While it is generally assumed that oysters reduce seston and phytoplankton concentrations, while ignoring biodeposits (Newell & Koch 2004), evidence that oyster reefs measurably reduce water column particulates or impact phytoplankton or microphytobenthic biomass or productivity (Plutchak et al. 2010) is generally lacking. Oyster-related seston decreases (interpreted as depletion) can be spatially variable (Grizzle et al. 2018), and the interplay between bottom shear stress with sediment and biodeposit resuspension and oysters suggests that observations should be interpreted with caution.

Phytoplankton did not shift to smaller cells in biodeposit tanks; however, this response did not include an assessment of picophytoplankton. Improved light penetration associated with oyster filtration (Newell & Koch 2004, Porter et al. 2004a) illuminates the surface of the sediment and alters sediment biogeochemical processes (Porter et al. 2004a). In this study, rather than promoting a phytoplankton bloom (Doering et al. 1986, Asmus & Asmus 1991, Souchu et al. 2001), particularly in oligotrophic systems (Cranford et al. 2007), oyster biodeposit addition and resuspension led to increased zooplankton populations, *A. tonsa*, and no phytoplankton bloom. Copepods play a key role in the food web as the main vector from the primary producers to higher trophic levels (Hansen et al. 1994, Verity & Smetacek 1996, Stibor et al. 2004a), while copepod chemical cues may have indirect cascading effects in plankton food webs (Grebner et al. 2019). Several potential connections between biode-

posit resuspension and both phytoplankton and zooplankton community structure are suggested from this study. Oyster biodeposits under these experimental conditions were funneled to higher trophic levels without negatively affecting water quality. In addition, diatoms with defenses may have important consequences on prey–predator relationships and on the biomass flux through marine food chains.

Acknowledgements. We thank the Maryland Sea Grant (grant no. SA75287870-E [R/P-62a]), the University of Baltimore Foundation for a Turner grant, and the NSF-sponsored Oyster Futures Program (OCE-1427019). Jay Horsey assisted throughout this experiment, Regina Minniss contributed numerous hours of zooplankton counts, Marcia Olson provided expert zooplankton identification, and Melanie Jackson and Michael Owens carried out biogeochemical flux experiments at the end of the STURM experiment. The Chesapeake Biological Laboratory and Horn Point Laboratory Analytical Services laboratories are thanked for sample analyses. We thank Kelton Clark for the use of his oysters, and the Patuxent Environmental and Aquatic Research Laboratory for providing space and research support throughout this study. Currently, the University of Baltimore operates the STURM facility through a cooperative arrangement with the Patuxent Environmental and Aquatic Research Laboratory (PEARL), Morgan State University. We also thank Amber DeMarr for help with the seawater system; 3 anonymous reviewers whose constructive criticism and detailed feedback improved the manuscript; and Samantha Dean for editorial feedback on this manuscript.

LITERATURE CITED

Adey WH, Loveland K (1998) Dynamic aquaria: building living ecosystems. Academic Press, San Diego, CA

Agusti S (1991) Allometric scaling of light absorption and scattering by phytoplankton cells. Can J Fish Aquat Sci 48:763–767

Ahlgren G, Gustafsson IB, Boberg M (1992) Fatty acid content and chemical composition of freshwater microalgae. J Phycol 28:37–50

Anderson TR, Martin AP, Lampitt RS, Trueman CN, Henson SA, Mayor DJ, Link J (2019) Quantifying carbon fluxes from primary production to mesopelagic fish using a simple food web model. ICES J Mar Sci 76:690–701

Armengol L, Franchy G, Ojeda A, Santana-del Pino Á, Hernández-León S (2017) Effects of copepods on natural microplankton communities: Do they exert top-down control? Mar Biol 164:136

Asmus RM, Asmus H (1991) Mussel beds: limiting or promoting phytoplankton? J Exp Mar Biol Ecol 148: 215–232

Ator SW, García AM, Schwarz GE, Blomquist JD, Sekellick AJ (2019) Toward explaining nitrogen and phosphorus trends in Chesapeake Bay tributaries, 1992–2012. J Am Water Resour Assoc 55:1149–1168

Ban S, Burns C, Castel J, Chaudron Y and others (1997) The paradox of diatom-copepod interactions. Mar Ecol Prog Ser 157:287–293

Behrenfeld MJ, Falkowski PG (1997) Photosynthetic rates derived from satellite-based chlorophyll concentration. Limnol Oceanogr 42:1–20

Berg JA, Newell RIE (1986) Temporal and spatial variations in the composition of seston available to the suspension feeder *Crassostrea virginica.* Estuar Coast Shelf Sci 23: 375–386

Bergkvist J, Thor P, Jakobsen HH, Waengberg SA, Selander E (2012) Grazer-induced chain length plasticity reduces grazing risk in a marine diatom. Limnol Oceanogr 57: 318–324

Berhane I, Sternberg RW, Kineke GC, Milligan TG, Kranck K (1997) The variability of suspended aggregates on the Amazon Continental Shelf. Cont Shelf Res 17:267–285

Bjærke O, Jonsson PR, Alam A, Selander E (2015) Is chain length in phytoplankton regulated to evade predation? J Plankton Res 37:1110–1119

Browning TJ, Al-Hashem AA, Hopwood MJ, Engel A, Wakefield ED, Achterberg EP (2019) Nutrient regulation of late spring phytoplankton blooms in the midlatitude North Atlantic. Limnol Oceanogr), doi:10.1002/lno.11376

Buchanan C, Lacouture RV, Marshall HG, Olson M, Johnson JM (2005) Phytoplankton reference communities for Chesapeake Bay and its tidal tributaries. Estuaries 28: 138–159

Budge SM, Parrish CC (1999) Lipid class and fatty acid composition of *Pseudo-nitzschia multiseries* and *Pseudo-nitzschia pungens* and effects of lipolytic enzyme deactivation. Phytochemistry 52:561–566

Calbet A (2001) Mesozooplankton grazing effect on primary production: a global comparative analysis in marine ecosystems. Limnol Oceanogr 46:1824–1830

Callier MD, Weise AM, McKindsey CW, Desrosiers G (2006) Sedimentation rates in a suspended mussel farm (Great-Entry Lagoon, Canada): biodeposit production and dispersion. Mar Ecol Prog Ser 322:129–141

Carlson DM (1978) The ecological role of zooplankton in a Long Island salt marsh. Estuaries 1:85–92

Chamberlain J, Fernandes TF, Read P, Nickell TD, Davies IM (2001) Impacts of biodeposits from suspended mussel (*Mytilus edulis* L.) culture on the surrounding surficial sediments. Biol Ocean Committee 58:411–416

Chen CC, Petersen JE, Kemp WM (1997) Spatial and temporal scaling of periphyton growth on walls of estuarine mesocosms. Mar Ecol Prog Ser 155:1–15

Clark DR, Flynn KJ, Owens NJP (2002) The large capacity for dark nitrate-assimilation in diatoms may overcome nitrate limitation on growth. New Phytol 155:101–108

Cloern JE (1982) Does the benthos control phytoplankton biomass in south San Francisco Bay? Mar Ecol Prog Ser 9:191–202

Cohen RRH, Dresler PV, Phillips EJP, Cory RL (1984) The effect of the Asiatic clam, *Corbicula fluminea*, on phytoplankton of the Potomac River, Maryland. Limnol Oceanogr 29:170–180

Colden AM, Fall KA, Cartwright GM, Friedrichs CT (2016) Sediment suspension and deposition across restored oyster reefs of varying orientation to flow: implications for restoration. Estuaries Coast 39:1435–1448

Cranford PJ, Strain PM, Dowd M, Hargrave BT, Grant J, Archambault MC (2007) Influence of mussel aquaculture on nitrogen dynamics in a nutrient enriched coastal embayment. Mar Ecol Prog Ser 347:61–78

d'Ippolito G, Romano G, Iadicicco O, Miralto A, Ianora A, Cimino G, Fontana A (2002) New birth-control alde-

hydes from the marine diatom *Skeletonema costatum*: characterization and biogenesis. Tetrahedron Lett 43: 6133–6136

Davis CS, Flierl GR, Wiebe PH, Franks PJS (1991) Micropatchiness, turbulence and recruitment in plankton. J Mar Res 49:109–151

Deason EE (1980) Grazing of *Acartia hudsonica* (*A. clausi*) on *Skeletonema costatum* in Narragansett Bay (USA): influence of food concentration and temperature. Mar Biol 60:101–113

Doering PH, Oviatt CA, Kelly JR (1986) The effects of the filter-feeding clam *Mercenaria mercenaria* on carbon cycling in experimental marine mesocosms. J Mar Res 44:839–861

Dower JF, Miller TJ, Leggett WC (1997) The role of microscale turbulence in the feeding ecology of larval fish. Adv Mar Biol 31:169–220

Droppo IG, Leppard GG, Flannigan DT, Liss SN (1997) The freshwater floc: a functional relationship of water and organic and inorganic constituents affecting suspended sediment properties. Water Air Soil Pollut 99:43–54

Durante G, Basset A, Stanca E, Roselli L (2019) Allometric scaling and morphological variation in sinking rate of phytoplankton. J Phycol 55:1386–1393

Estrada M, Berdalet E (1997) Phytoplankton in a turbulent world. Sci Mar 61:125–140

Faubel A (1982) Determination of individual meofauna dry weight values in relation to definite size classes. Cah Biol Mar 23:339–345

Finkel ZV, Irwin AJ (2000) Modeling size-dependent photosynthesis: light absorption and the allometric rule. J Theor Biol 204:361–369

Finkel ZV, Irwin AJ, Schofield O (2004) Resource limitation alters the 3/4 size scaling of metabolic rates in phytoplankton. Mar Ecol Prog Ser 273:269–279

Fisher TR, Peele ER, Ammerman JW, Harding LW Jr (1992) Nutrient limitation of phytoplankton in Chesapeake Bay. Mar Ecol Prog Ser 82:51–63

Fisher TR, Gustafson AB, Sellner KG, Lacouture R and others (1999) Spatial and temporal variation of resource limitation in Chesapeake Bay. Mar Biol 133:763–778

Fouilland E, Mostajir B, Gosselin M, Levasseur M and others (2016) Effect of mixing on the structure of a natural plankton community: a mesocosm study. Vie Milieu 66: 251–259

Fridolfsson E, Lindehoff E, Legrand C, Hylander S (2018) Thiamin (vitamin B1) content in phytoplankton and zooplankton in the presence of filamentous cyanobacteria. Limnol Oceanogr 63:2423–2435

Gárate-Lizárraga I, Esqueda-Escárcega GM (2016) Proliferation of *Falcula hyalina* and *Cylindrotheca closterium* (Bacillariophyceae) on copepods in Bahía de La Paz, Gulf of California, Mexico. Rev Biol Mar Oceanogr 51: 197–201

Gerhard M, Koussoroplis AM, Hillebrand H, Striebel M (2019) Phytoplankton community responses to temperature fluctuations under different nutrient concentrations and stoichiometry. Ecology 100:e02834

Giles H, Pilditch CA (2004) Effect of diets on sinking rates and erosion thresholds of mussel *Perna canaliculus* biodeposits. Mar Ecol Prog Ser 282:205–219

Gliwicz ZM, Siedlar E (1980) Food size limitation and algae interfering with food collection in *Daphnia.* Arch Hydrobiol 88:155–177

Goodman KS (1980) The estimation of individual dry weight and standing crop of harpacticoid copepods. Hydrobiologia 72:253–259

Grebner W, Berglund EC, Berggren F, Eklund J, Harðadóttir S, Andersson MX, Selander E (2019) Induction of defensive traits in marine plankton—new copepodamide structures. Limnol Oceanogr 64:820–831

Grizzle RE, Rasmussen A, Martignette AJ, Ward K, Coen LD (2018) Mapping seston depletion over an intertidal eastern oyster (*Crassostrea virginica*) reef: implications for restoration of multiple habitats. Estuar Coast Shelf Sci 212:265–272

Guadayol O, Peters F, Marrasé C, Gasol JM and others (2009) Episodic meteorological and nutrient-load events as drivers of coastal planktonic ecosystem dynamics: a time-series analysis. Mar Ecol Prog Ser 381:139–155

Gust G (1988) Skin friction probes for field applications. J Geophys Res 93:14121–14132

Hansen B, Bjornsen PK, Hansen PJ (1994) The size ratio between planktonic predators and their prey. Limnol Oceanogr 39:395–403

Harding LW Jr, Mallonee ME, Perry ES, Miller WD, Adolf JE, Gallegos CL, Paerl HW (2019) Long-term trends, current status, and transitions of water quality in Chesapeake Bay. Sci Rep 9:6709

Harley CDG, Connell SD, Doubleday ZA, Kelaher B, Russell BD, Sara G, Helmuth B (2017) Conceptualizing ecosystem tipping points within a physiological framework. Ecol Evol 7:6035–6045

Harvey HW, Cooper LHN, Lebour MV, Russell FS (1935) Plankton production and its control. J Mar Biol Assoc UK 20:407–441

Haven DS, Morales-Alamo R (1970) Filtration of particles from suspension by the American oyster *Crassostrea virginica.* Biol Bull (Woods Hole) 139:248–264

Hessen DO, Van Donk E (1993) Morphological changes in *Scenedesmus* induced by substances released from *Daphnia.* Arch Hydrobiol 127:129–140

Hildreth DJ (1980) Bioseston production by *Mytilus edulis* and its effect in experimental systems. Mar Biol 55: 309–315

Iversen KR, Primicerio R, Larsen A, Egge JK and others (2010) Effects of small-scale turbulence on lower trophic levels under different nutrient conditions. J Plankton Res 32:197–208

Jeffrey SW, Vesk M (1997) Introduction to marine phytoplankton and their pigment structures. In: Jeffrey SW, Mantoura RFC, Wright SW (eds) Phytoplankton pigments in oceanography: guidelines to modern methods. Vol 10. Monographs on oceanographic methodology. UNESCO Publishing, Paris, p 74–75

Jiang Z, Du P, Liao Y, Liu Q and others (2019) Oyster farming control on phytoplankton bloom promoted by thermal discharge from a power plant in a eutrophic, semi-enclosed bay. Water Res 159:1–9

Jónasdóttir SH, Kiørboe T, Tang KW, St. John M, Visser AW, Saiz E, Dam HG (1998) Role of diatoms in copepod production: good, harmless or toxic? Mar Ecol Prog Ser 172:305–308

Jordan SJ (1987) Sedimentation and remineralization associated with biodeposition by the American oyster *Crassostrea virginica.* PhD dissertation, University of Maryland, College Park, MD

Kamp A, Hogslund S, Risgaard-Petersen N, Stief P (2015) Nitrate storage and dissimilatory nitrate reduction by eukaryotic microbes. Front Microbiol 6:1492

Kang Y, Song X, Liu Z (2013) Sediment resuspension dampens the effect of nutrient inputs on the phytoplankton community: a mesocosm experiment study. Hydrobiologia 710:117–127

Kellogg ML, Cornwell JC, Owens MS, Paynter KT (2013) Denitrification and nutrient assimilation on a restored oyster reef. Mar Ecol Prog Ser 480:1–19

Kiørboe T (1993) Turbulence, phytoplankton cell size, and the structure of pelagic food webs. Adv Mar Biol 29:1–72

La Rosa T, Mirto S, Favaloro E, Savona B, Sará G, Danovaro R, Mazzola A (2002) Impact on the water column biochemistry of a Mediterranean mussel and fish farm. Water Res 36:713–721

Lacouture RV (2010) Quality assurance documentation plan for the Maryland phytoplankton component of the Chesapeake Bay water quality monitoring program. Report prepared for the Maryland Department of Natural Resources by the Morgan State University Estuarine Research Center. https://www.chesapeakebay.net/documents/3684/md_phytoplankton_qapp_2009-2010.pdf

Lawrence D, Dagg MJ, Liu H, Cummings SR, Ortner PB, Kelble C (2004) Wind events and benthic–pelagic coupling in a shallow subtropical bay in Florida. Mar Ecol Prog Ser 266:1–13

Lebour MV (1922) The food of plankton organisms. J Mar Biol Assoc UK 12:644–677

Lomas MW, Glibert PM (2000) Comparisons of nitrate uptake, storage and reduction in marine diatoms and flagellates. J Phycol 36:903–913

Lund EJ (1957) Self silting, survival of the oyster as a closed system and reducing tendencies of the environment of the oyster. Publ Inst Mar Sci Univ Tex 4:313–319

MacIsaac EA, Stockner JG (1993) Enumeration of phototrophic picoplankton by autofluorescence microscopy. In: Kemp PF, Sherr BF, Sherr EB, Cole JJ (eds) Handbook of methods in aquatic microbial ecology. Lewis Publishers, Boca Raton, FL, p 187–197

Marshall HG (1994) Chesapeake Bay phytoplankton. I. Composition. Proc Biol Soc Wash 107:573–585

Marshall HG, Alden RW (1990) Spatial and temporal diatom assemblages and other phytoplankton within the lower Chesapeake Bay, USA. In: Simola H (ed) Proceedings of the 10th International Diatom Symposium. Koeltz Scientific Books, Koenigstein, p 311–322

Marshall HG, Burchardt L, Lacouture R (2005) A review of phytoplankton composition within Chesapeake Bay and its tidal estuaries. J Plankton Res 27:1083–1102

Martin JH (1970) Phytoplankton-zooplankton relationships in Narragansett Bay. VI. The seasonal importance of grazing. Limnol Oceanogr 15:413–418

Martin-Jézéquel V, Hildebrand M, Brzezinski MA (2000) Silicon metabolism in diatoms: implications for growth. J Phycol 36:821–840

Mazur-Marzec H, Bertos-Fortis M, Toruńska-Sitarz A, Fidor A, Legrand C (2016) Chemical and genetic diversity of *Nodularia spumigena* from the Baltic Sea. Mar Drugs 14: 209

McLean K, Stone M, Droppo IG, Smith R (2018) Erodibility and transport behavior of dreissenid mussel deposits in an annular flume. J Soils Sediments 18:3448–3462

Medina-Gómez I, Trujillo AA, Marino-Tapia I, Cruz G, Herrera-Silveira J, Enriquez C (2019) Phytoplankton responses under a joint upwelling event and an algal bloom scenario in the southeast Gulf of Mexico. Cont Shelf Res 184:30–43

Miralto A, Barone G, Romano G, Poulet SA and others (1999) The insidious effect of diatoms on copepod reproduction. Nature 402:173–176

Morin J, Morse JW (1999) Ammonium release from resuspended sediments in the Laguna Madre estuary. Mar Chem 65:97–110

Murphy RR, Perry E, Harcum J, Keisman J (2019) A generalized additive model approach to evaluating water quality: Chesapeake Bay case study. Environ Model Softw 118:1–13

Newell RIE (1988) Ecological changes in Chesapeake Bay: Are they the result of overharvesting the American oyster, *Crassostrea virginica*? In: Lynch MP, Krome EC (eds) Understanding the estuary: advances in Chesapeake Bay research. Publication 129 (CBP/TRS 24/88). Chesapeake Research Consortium, Gloucester Point, VA, p 536–546

Newell RIE, Koch EW (2004) Modeling seagrass density and distribution in response to changes in turbidity stemming from bivalve filtration and seagrass sediment stabilization. Estuaries 27:793–806

Newell RIE, Fisher TR, Holyoke RR, Cornwell JC (2005) Influence of eastern oysters on nitrogen and phosphorus regeneration in Chesapeake Bay, USA. In: Dame RF, Olenin S (eds) The comparative roles of suspension feeders in ecosystems, Book 47. Kluwer, Dordrecht, p 93–120

O'Connors HB, Biggs DC, Ninivaggi DV (1980) Particle-size-dependent maximum grazing rates for *Temora longicornis* fed natural particle assemblages. Mar Biol 56:65–70

Olson MB, Lessard EJ, Wong CHJ, Bernhardt MJ (2006) Copepod feeding selectivity on microplankton, including the toxigenic diatoms *Pseudo-nitzschia* spp., in the coastal Pacific Northwest. Mar Ecol Prog Ser 326: 207–220

Pančić M, Kiørboe T (2018) Phytoplankton defence mechanisms: traits and trade-offs. Biol Rev Camb Philos Soc 93: 1269–1303

Parsons TR, Maita Y, Lalli CM (1984) A manual of chemical and biological methods for seawater analysis. Pergamon, Oxford University Press, Oxford

Peters F, Marrasé C (2000) Effects of turbulence on plankton: an overview of experimental evidence and some theoretical considerations. Mar Ecol Prog Ser 205: 291–306

Petersen JE, Sanford LP, Kemp WM (1998) Coastal plankton responses to turbulent mixing in experimental ecosystems. Mar Ecol Prog Ser 171:23–41

Plutchak R, Major K, Cebrian J, Foster CD and others (2010) Impacts of oyster reef restoration on primary productivity and nutrient dynamics in tidal creeks of the north central Gulf of Mexico. Estuaries Coasts 33:1355–1364

Pohnert G (2005) Diatom/copepod interactions in plankton: the indirect chemical defense of unicellular algae. ChemBioChem 6:946–959

Pohnert G, Lumineau O, Cueff A, Adolph S, Cordevant C, Lange M, Poulet S (2002) Are volatile unsaturated aldehydes from diatoms the main line of chemical defence against copepods? Mar Ecol Prog Ser 245:33–45

Poikane S, Kelly MG, Salas Herrero F, Pitt JA and others (2019) Nutrient criteria for surface waters under the European Water Framework Directive: current state-of-the-art, challenges and future outlook. Sci Total Environ 695:133888

Porter ET, Cornwell JC, Sanford LP (2004a) Effect of oysters

Crassostrea virginica and bottom shear velocity on benthic–pelagic coupling and estuarine water quality. Mar Ecol Prog Ser 271:61–75

Porter ET, Sanford LP, Gust G, Porter FS (2004b) Combined water-column mixing and benthic boundary-layer flow in mesocosms: key for realistic benthic–pelagic coupling studies. Mar Ecol Prog Ser 271:43–60

Porter ET, Owens MS, Cornwell JC (2006) Effect of sediment manipulation on the biogeochemistry of experimental sediment systems. J Coast Res 22:1539–1551

Porter ET, Mason RP, Sanford LP (2010) Effect of tidal resuspension on benthic–pelagic coupling in an experimental ecosystem study. Mar Ecol Prog Ser 413:33–53

Porter ET, Mason RP, Sanford LP (2013) Effects of shear stress and hard clams on seston, microphytobenthos, and nitrogen dynamics in mesocosms with tidal resuspension. Mar Ecol Prog Ser 479:25–45

Porter ET, Franz H, Lacouture R (2018a) Impact of Eastern oyster *Crassostrea virginica* biodeposit resuspension on the seston, nutrient, phytoplankton, and zooplankton dynamics: a mesocosm experiment. Mar Ecol Prog Ser 586:21–40

Porter ET, Sanford LP, Porter FS, Mason RP (2018b) STURM: resuspension mesocosms with realistic bottom shear stress and water column turbulence for benthic-pelagic coupling studies: design and applications. J Exp Mar Biol Ecol 499:35–50

Ray NE, Li J, Kangas PC, Terlizzi DE (2015) Water quality upstream and downstream of a commercial oyster aquaculture facility in Chesapeake Bay, USA. Aquacult Eng 68:35–42

Riegman R, Kuipers BR, Noordeloos AAM, Witte HJ (1993) Size-differential control of phytoplankton and the structure of plankton communities. Neth J Sea Res 31: 255–265

Sanford LP (1997) Turbulent mixing in experimental ecosystems. Mar Ecol Prog Ser 161:265–293

Sarthou G, Timmermans KR, Blain S, Tréguer P (2005) Growth physiology and fate of diatoms in the ocean: a review. J Sea Res 53:25–42

Scholes RJ, Kruger JM (2011) A framework for deriving and triggering thresholds for management intervention in uncertain, varying and time-lagged systems. Koedoe 53: Art#987

Schulte DM, Burke RP (2014) Recruitment enhancement as an indicator of oyster restoration success in Chesapeake Bay. Ecol Restor 32:434–440

Shimeta J, Amos CL, Beaulieu SE, Katz SL (2003) Resuspension of benthic protists at subtidal coastal sites with differing sediment composition. Mar Ecol Prog Ser 259: 103–115

Smayda TJ (1974) Some experiments on the sinking characteristics of two freshwater diatoms. Limnol Oceanogr 19: 628–635

Smayda TJ (1978) From phytoplankters to biomass. In: Sournia A (ed) Phytoplankton manual. United Nations Educational, Scientific and Cultural Organization, Paris, p 273–279

Smayda TJ, Bienfang PK (1983) Suspension properties of various phyletic groups of phytoplankton and tintinnids in an oligotrophic subtropical system. Mar Ecol 4:289–300

Smayda TJ, Boleyn BJ (1966) Experimental observations on the flotation of marine diatoms. II *Skeletonema costatum* and *Rhizosolenia setigera*. Limnol Oceanogr 11:18–34

Souchu P, Vaquer A, Collos Y, Landrein S, Deslous-Paoli JM, Bibent B (2001) Influence of shellfish farming activities on the biogeochemical composition of the water column in Thau lagoon. Mar Ecol Prog Ser 218:141–152

Sprung M (1984) Physiological energetics of mussel larvae (*Mytilus edulis*). I. Shell growth and biomass. Mar Ecol Prog Ser 17:283–293

Stibor H, Vadstein O, Diehl S, Gelzleichter A and others (2004) Copepods act as a switch between alternative trophic cascades in marine pelagic food webs. Ecol Lett 7:321–328

Strathmann RR (1967) Estimating the organic carbon content of phytoplankton from cell volume or plasma volume. Limnol Oceanogr 12:411–418

Su J, Tian T, Krasemann H, Schartau M, Wirtz K (2015) Response patterns of phytoplankton growth to variations in resuspension in the German Bight revealed by daily MERIS data in 2003 and 2004. Oceanologia 57:328–341

Sutula M, Kudela R, Hagy JD 3rd, Harding LW Jr and others (2017) Novel analyses of long-term data provide a scientific basis for chlorophyll-a thresholds in San Francisco Bay. Estuar Coast Shelf Sci 197:107–118

Takabayashi M, Lew K, Johnson A, Marchi AL, Dugdale R, Wilkerson FP (2006) The effect of nutrient availability and temperature on chain length of the diatom, *Skeletonema costatum*. J Plankton Res 28:831–840

Tennekes H, Lumley JL (1972) A first course in turbulence. MIT Press, Cambridge, MA

Testa JM, Brady DC, Cornwell JC, Owens MS and others (2015) Modeling the impact of floating oyster (*Crassostrea virginica*) aquaculture on sediment–water nutrient and oxygen fluxes. Aquacult Environ Interact 7:205–222

Turner JT, Bruno SF, Larson RJ, Staker D, Sharma GM (1983) Seasonality of plankton assemblages in a temperate estuary. Mar Ecol 4:81–99

Utermöhl H (1958) Zur Vervollkommnung der quantitativen Phytoplankton-Methodik. Mitt Int Ver Theor Angew Limnol 9:1–38

Vadstein O, Stibor H, Lippert B, Løseth K, Roederer W, Sundth-Hansen L, Olsen Y (2004) Moderate increase in the biomass of omnivorous copepods may ease grazing control of planktonic algae. Mar Ecol Prog Ser 270: 199–207

Van Donk E, Ianora A, Vos M (2011) Induced defences in marine and freshwater phytoplankton: a review. Hydrobiologia 668:3–19

Van Heukelem L, Thomas CS (2001) Computer-assisted high-performance liquid chromatography method development with applications to the isolation and analysis of phytoplankton pigments. J Chromatogr A 910:31–49

Van Meerssche E, Pinckney JL (2019) Nutrient loading impacts on estuarine phytoplankton size and community composition: community-based indicators of eutrophication. Estuaries Coasts 42:504–512

Veldhuis MJW, Kraay GW (2000) Application of flow cytometry in marine phytoplankton research: current applications and future perspectives. Sci Mar 64:121–134

Verity PG, Smetacek V (1996) Organism life cycles, predation, and the structure of marine pelagic ecosystems. Mar Ecol Prog Ser 130:277–293

Villamaña M, Marañón E, Cermeño P, Estrada M and others (2019) The role of mixing in controlling resource availability and phytoplankton community composition. Prog Oceanogr 178:102181

Waite A, Fisher A, Thompson PA, Harrison PJ (1997) Sinking rate versus cell volume relationships illuminate sink-

ing rate control mechanisms in marine diatoms. Mar Ecol Prog Ser 157:97–108

Walker TR, Grant J, Hill PS, Cranford PJ, Lintern G, Scofield B (2005) Measuring particle dynamics in arctic and mussel aquaculture environments. Proceedings of the 12th Canadian Coastal Conference/Comptes-rendus, Conférence canadienne sur le littoral 2005. Canadian Coastal Science and Engineering Association, Ottawa, p 1–11

White JR, Roman MR (1992) Seasonal study of grazing by metazoan zooplankton in the mesohaline Chesapeake Bay. Mar Ecol Prog Ser 86:251–261

Widdows J, Brinsley M (2002) Impact of biotic and abiotic processes on sediment dynamics and the consequences to the structure and functioning of the intertidal zone. J Sea Res 48:143–156

Widdows J, Brinsley M, Elliott M (1998) Use of *in situ* flume to quantify particle flux (biodeposition rates and sediment erosion) for an intertidal mudflat in relation to changes in current velocity and benthic macrofauna. In: Black KS, Paterson DM, Cramp A (eds) Sedimentary processes in the intertidal zone, Book 139. The Geological Society, Bath, p 85–97

Williamson TR, Tilley DR, Campbell E (2015) Emergy analysis to evaluate the sustainability of two oyster aquaculture systems in the Chesapeake Bay. Ecol Eng 85: 103–120

Wirtz KW, Pahlow M (2010) Dynamic chlorophyll and nitrogen:carbon regulation in algae optimizes instantaneous growth rate. Mar Ecol Prog Ser 402:81–96

Wood JD, Elliott D, Garman G, Hopler D and others (2016) Autochthony, allochthony and the role of consumers in influencing the sensitivity of aquatic systems to nutrient enrichment. Food Webs 7:1–12

Wootton JT (2002) Indirect effects in complex ecosystems: recent progress and future challenges. J Sea Res 48: 157–172

Yallop ML, de Winder B, Paterson DM, Stal LJ (1994) Comparative structure, primary production and biogenic stabilization of cohesive and non-cohesive marine sediments inhabited by microphytobenthos. Estuar Coast Shelf Sci 39:565–582

Ziervogel K, Forster S (2005) Aggregation and sinking behaviour of resuspended fluffy layer material. Cont Shelf Res 25:1853–1863

Editorial responsibility: Steven Lohrenz, New Bedford, Massachusetts, USA

Submitted: September 10, 2019; Accepted: February 27, 2020
Proofs received from author(s): April 10, 2020